MEEN 626 – Lubrication Theory

Semester Project
Comparison of Experimental and Numerical Results of Various 3D Printed Bearing Designs

Dung Tran

Jitaditya Mondal

Jonathan Thiele

Metapun Nuntakulamarat

Nathan Eitrheim

Submission Date: 05 December 2016

Instructors: Dr. Luis San Andrés

Executive Summary

The objective of this study is to compare experimental and numerical results of various 3D printed bearing designs. To achieve this objective, Bentley Nevada rotor kit provides experimental results, which are then compared with predications obtained from XLTRC^2 software.

In this study, three different bearing designs are considered: Plain Journal, Pressure Dam and Flexure Pivot Bearing. Using existing print options available within Texas A&M campus, four bearing configurations are printed. The material and printing technique used are shown below in Table 1.

Table 1: Varying Bearings

	Bearing	**Material**	**Printing technique**
1	Flexure Pivot (PLA)	PLA	Fused Deposition Modelling
2	Flexure Pivot (Photopolymer)	Photopolymer	Polyjet
3	Plain Journal Bearing (Photopolymer)	Photopolymer	Polyjet
4	Pressure Dam Bearing (Photopolymer)	Photopolymer	Polyjet

These bearings are tested and documented for their static performance, temperature rise, and flow rate. These static experimental values are compared against XLTRC^2 predictions. Using ADRE software, coupled with the proximity probes, waterfall charts, synchronous vibration and orbit plots are generated for the bearings. These bearing plots provide insights into dynamic performance and probable instability. The report concludes with various recommendations and future work within this area.

Contents

Executive Summary i

List of Figures iii

List of Tables v

I. Introduction 1

II. Description of Bentley Nevada rotor kit 3

III. Bearing Selection 4

Pressure Dam Bearing 4

Flexure Pivot Bearing 5

Summary of bearing selection 6

IV. Solidworks models 7

Solidworks model of bearings 7

Solidworks model of bearing housing 8

V. 3D Printing Options 10

3D printing using Polyjet technique (High Fidelity) 10

3D printing using Fused Deposition Modelling (Low Fidelity) 11

VI. 3D print outputs 13

3D printed bearing housing 13

3D printed bearings 14

VII. Experiment and Validation of Bearing Performance 15

Test setup description 15

Measuring devices 16

Testing procedure 17

Proximity probe calibration procedure 17

Load adjustment procedure 17

Description of each test run 19

VIII. Results and Discussion 20

Static Predictions and Results 20

Dynamic Results 22

IX. Recommendations 30
X. Future Work 32
XI. Conclusion 33
References 35
Appendix 37
A. ISO VG 32 Properties 37
B. Probe calibration 38

List of Figures

Figure 1 3D printed aluminum bearings [2] 1
Figure 2 3D printed gyroscopic bearings [1] 1
Figure 3 Bentley Nevada rotor kit 3
Figure 4 Schematic of pressure dam bearings [5] 4
Figure 5 Flexure pivot bearing schematic 5
Figure 6 Plain Journal Bearing 7
Figure 7 Pressure Dam Bearing Model 7
Figure 8 Pressure Dam Bearing Inner Diameter Layout 7
Figure 9 Flex Pivot Bearing Sketch 8
Figure 10 Flex Pivot Bearing Model 8
Figure 11 Initial Bearing housing 8
Figure 12 Annotated diagram of the bearing housing 9
Figure 13 Polyjet printing technique [10] 10
Figure 14 FDM printing technique [11] 11
Figure 15 Annotated diagram of the 3D printed bearing housing 13
Figure 16 3D printed bearings 14
Figure 17 Final test setup 15
Figure 18 Measuring devices 16
Figure 19 Setup of voltmeter 17
Figure 20 Checking travelling gap 17
Figure 21 Setup of dial gauge 18
Figure 22 Removal of bearing housing 18
Figure 23 Adjusting spring to the required load 18
Figure 24 Confirming static load with hanging scale 18
Figure 25 Confirming rotor position using dial gauge 19

Figure 26 Plain journal bearing measured and predicted oil flow rates 20
Figure 27 Plain journal bearing measured and predicted temperature rise 20
Figure 28 Pressure dam bearing measured and predicted oil flow rates 21
Figure 29 Pressure dam bearing measured and predicted temperature rise 21
Figure 30: PLA Flexure pivot bearing - Bode plot at 0N load 23
Figure 31: Photopolymer flexure pivot bearing - Bode plot at 0N load 23
Figure 32: PLA Flexure pivot bearing - Bode plot at 2N load 23
Figure 33: Photopolymer flexure pivot bearing - Bode plot at 2N load 23
Figure 34: PLA Flexure pivot bearing - Bode plot at 4N load 23
Figure 35: Photopolymer flexure pivot bearing - Bode plot at 4N load 23
Figure 36: PLA Flexure pivot bearing - Bode plot at 6.58N load 24
Figure 37: Photopolymer flexure pivot bearing - Bode plot at 6.58N load 24
Figure 38: PLA Flexure pivot bearing - Cascade plot at 0N load 24
Figure 39: Photopolymer flexure pivot bearing - Cascade plot at 0N load 24
Figure 40: PLA Flexure pivot bearing - Cascade plot at 2N load 24
Figure 41: Photopolymer flexure pivot bearing - Cascade plot at 2N load 24
Figure 42: PLA Flexure pivot bearing - Cascade plot at 4N load 25
Figure 43: Photopolymer flexure pivot bearing - Cascade plot at 4N load 25
Figure 44: PLA Flexure pivot bearing - Cascade plot at 6.58N load 25
Figure 45: Photopolymer flexure pivot bearing - Cascade plot at 6.58N load 25
Figure 46: Bearing vibration comparison at 2000rpm 26
Figure 47: Bearing vibration comparison at 5000rpm 26
Figure 48: Bearing vibration comparison at 8000rpm 26
Figure 49: Bearing vibration comparison at critical speed 26
Figure 50: Plain journal bearing - Bode plot at 0N load 27
Figure 51: Pressure dam bearing - Bode plot at 0N load 27
Figure 52: Plain journal bearing - Bode plot at 2N load 27
Figure 53: Pressure dam bearing - Bode plot at 2N load 27
Figure 54: Plain journal bearing - Bode plot at 4N load 27
Figure 55: Pressure dam bearing - Bode plot at 4N load 27
Figure 56: Plain journal bearing - Bode plot at 6.58N load 27
Figure 57: Pressure dam bearing - Bode plot at 6.58N load 27
Figure 58: Plain journal bearing - Cascade plot at 0N load 28
Figure 59: Pressure dam bearing - Cascade plot at 0N load 28
Figure 60: Plain journal bearing - Cascade plot at 2N load 28
Figure 61: Pressure dam bearing - Cascade plot at 2N load 28
Figure 62: Plain journal bearing - Cascade plot at 4N load 28

Figure 63: Pressure dam bearing - Cascade plot at 4N load 28
Figure 64: Plain journal bearing - Cascade plot at 6.5N load 28
Figure 65: Pressure dam bearing - Cascade plot at 6.5N load 28
Figure 66: Centerline plot for the plain journal bearing operating at 6.58N load 29
Figure 67: Centerline plot for the pressure dam bearing operating at 6.58N load 29
Figure 68 Annotated diagram of new bearing housing 30
Figure 69 ISO VG 32 properties (taken from Chevron Data sheet) 37

List of Tables

Table 1: Varying Bearings i
Table 2 Important dimensions of the Bentley Nevada Rotor kit 3
Table 3 Intended dimensions of test bearings 6
Table 4 Specification of high fidelity printer 11
Table 5 Specification of low fidelity printer 12
Table 6 Final clearance of the bearings 14
Table 7 Test Matrix 15
Table 8: Precision of measuring instruments 16
Table 9: Summary of bearing performance 22

I. Introduction

Many Original Equipment Manufacturers (OEMs) of rotating equipment include bearing selection in the last stage of their design stage. If proper bearing selection is not performed, excessive vibrations and instability might become a concern for the machine. These OEMs increasingly outsource bearings to push the machine's boundaries of operating conditions. To meet needs, bearing manufacturers develop several designs and run various iterations. Conventional manufacturing techniques, such as using a milling, lathe, or even CNC machines, require expertise and acquires time to undergo manufacturing iterations. Additive manufacturing, 3D printing, provides an alternative solution for easy and fast production for design iterations and holds potential for bearing mass production.

There are multiple advantages to 3D printing. The first advantage is that a 3D printer can be operated with minimal experience. 3D printing softwares have made 3D printing very user-friendly and easy to learn. Secondly, bearings can be produced rapidly compared to conventional lathe machines or CNC tools. Thirdly, 3D printers allow the production of complex structures which are not possible using conventional manufacturing techniques or would take time and effort. Two examples are presented in this regard. Figure 1 shows an 3D printed aluminum bearing with internal honeycomb structure to make it more lightweight, yet very strong [2]. Figure 2 shows a gyroscopic ball bearing printed very easily through a 3D printer [1].

Figure 1 3D printed aluminum bearings [2]

Figure 2 3D printed gyroscopic bearings [1]

However, the 3D printing process has a few disadvantages. 3D printing processes primarily use plastic. There have been a few ventures into 3D metal printing but it still has not become mainstream and available to public. The second disadvantage is that 3D printing is limited to small scale production and mass production is still not very feasible using 3D printers [3]. Thirdly, 3D printing is precise but not accurate. Thus, a few iterations are needed to obtain desired accuracy. Thus, few iterations are needed to obtain desired accuracy.

Although 3D printing has drawbacks, it is safe to say the future to bearing manufacturing is additive manufacturing. Moving toward this direction, the project applies the 3D printing technology to bearings.

The objective in this project is to compare lubrication experimental results with three different 3D printed bearing designs to numerical predictions. A plane journal, pressure dam, and a flexure pivot bearing are designed and manufactured for this project with a bearing housing for easy replacement and installation on the test rig. The bearings and housing are modeled in Solidworks® and manufactured with 3D printing techniques out of polymer. Bearing surfaces are printed oversized and sanded to final clearance; this results with the desired clearance and a smooth surface finish. Each bearing is tested on a Bentley Nevada rotor kit. Numerical predictions using the bearing codes in the rotordynamic software suite XLTRC2® are compared to the experimental results.

II. Description of Bentley Nevada rotor kit

The Bentley Nevada rotor kit located at the Texas A&M University Turbomachinery Laboratory is shown in Figure 3. A variable speed motor drives the shaft supported by a bushing on the drive side and the bearing on the non-drive end. Four proximity sensors measure shaft position at both drive, and non-drive ends in the horizontal and vertical directions. Load is optionally adjusted by a spring attached to a rolling element bearing on the shaft. The imbalance can be changed by placing weights in the balance wheel. Oil into the bearing is gravity fed from the reservoir. There is a sump which collects the oil that flows out of the bearing. Some dimensions of the kit are mentioned below in Table 2.

Table 2 Important dimensions of the Bentley Nevada Rotor kit

Shaft diameter (D)	24.70 mm (0.9724 inch)
Bearing axial length (L)	14.22 mm (0.56 in)
L/D ratio	0.58
Radial clearance (c)	191 microns (7.5 mils)

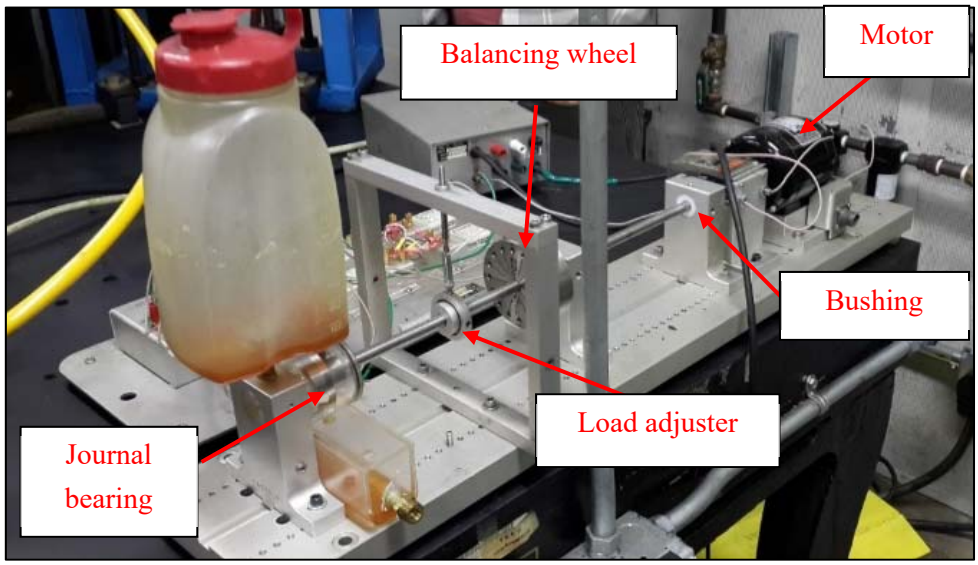

Figure 3 Bentley Nevada rotor kit

III. Bearing Selection

Three different bearings were considered for 3D printing: Plain journal, pressure dam, and flexure pivot bearing. Literature review provided optimum design dimensions for the pressure dam and flexure pivot bearing. However, all the bearings were made to have an 0.56" axial length to maintain an L/D ratio of 0.58, as that of the original plain journal bearing. Another point to note about clearance to the 3D printed bearings, is they're chosen to have a 4 mil radial clearance, because it deemed reasonable rather than existing clearance of 7.5 mils.

Pressure Dam Bearing

The schematic of pressure dam bearing is shown in Figure 4. There are 4 design parameters that can be changed in the geometry of a pressure dam bearing:

- Film Thickness ratio (h_1/h_2)
- Axial dam length ratio (L_d/L)
- Relief track length ratio (L_t/L)
- Dam location (θ_s)

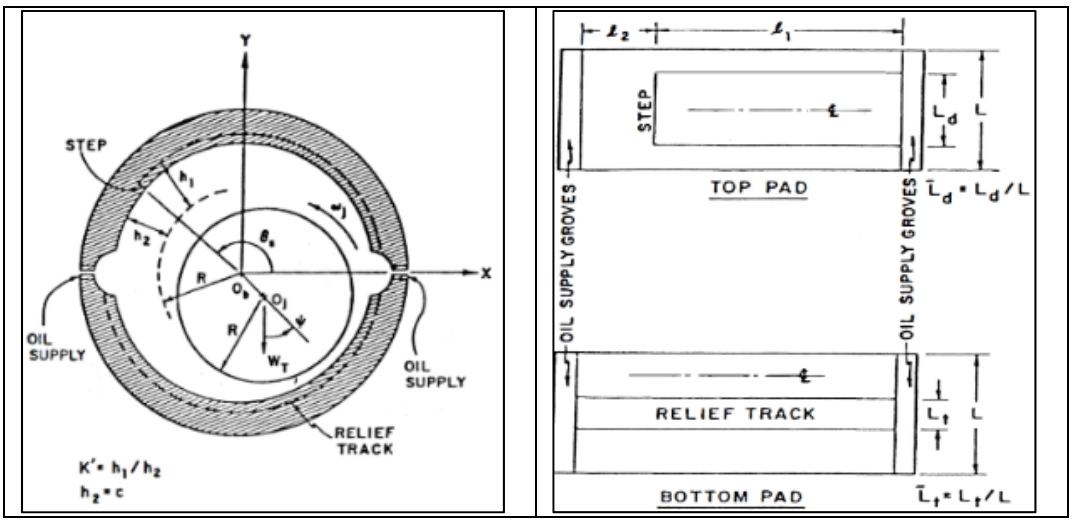

Figure 4 Schematic of pressure dam bearings [5]

Allaire et al. mentions optimum film thickness ratio for optimum load capacity is 3.0 [4]. However, in stability terms, a film thickness ratio of 6.0 is considered optimum [5]. For the project, a film thickness ratio of 4.0 was chosen, between the two different optimum values. In pressure dam bearings, relief track adds stability at low sommerfeld numbers [6]. Allaire et al. shows that a relief track length ratio of 0.5 gives highest stability. Surveying literature, the common axial dam length ratio was found to be 0.75 and for the experiments, it was chosen to be 0.7 [5,6].

Flexure Pivot Bearing

Flexure pivot bearings uses a layout similar to tilting pad bearings with circumferential pads enclosing the journal, though the movement doesn't involve a ball bearing nor rocker. The pads are fixed on a stem providing a rigid structure similar to the flag pole that flexes or deflects due to drag forces on the flag. The pylon stretches from within the bearing material and connects to the bearing pad. Because the pad is connected or physically connected to the web column, there is no wear underneath pad from constant rubbing. Nor misalignment installations as the manufacturing process includes constructing both stem and pad in one sitting to the bearing. This mitigates almost all tolerance issues, where the film thickness is a crucial design parameter. Comparing to tilting pad bearings, the flex pivot is easier to install into the housing as there is no further prepping. As in connecting pad, ball pivot, hex key screw support for pivot. Nor any small installation involving tilting pad bearing. This provides flex pivot bearings lasting life cycles in operation as there is no wear in material within the web structure. There is also very small movement as the web structure comes with radial stiffness where the tilting pad has no restricting forces from rocking. Figure 5 shows the schematic of a flexure pivot bearing.

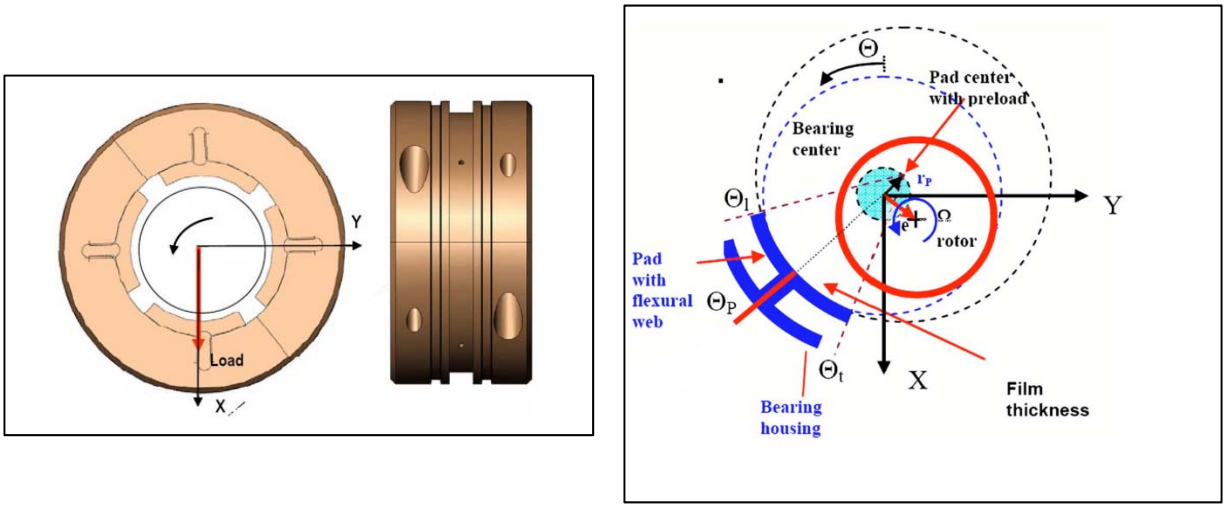

Figure 5 Flexure pivot bearing schematic

For the offset, 0.6 was chosen, following the choice of offset present on a paper where FPTPB is used for micro-turbomachinery applications [7]. For any tiling pad bearing there follows two orientations, load between pad and load on pad configurations. The latter provides higher bearing stiffness with increase in journal speed. Both configurations have similar vertical stiffness ratio and optimum damping ratio [8].

Summary of bearing selection

The summary of this section is presented in Table 3.

Table 3 Intended dimensions of test bearings

Plain Journal Bearing	Pressure Dam Bearing	Flexure Pivot Bearing
- Clearance = 0.102 mm (4 mil)	- Clearance = 0.102 mm (4 mil) - Film Thickness ratio, $h_1/h_2 = 6$ - Axial dam length ratio, $L_d/L = 0.7$ - Relief track length ratio, $L_t/L = 0.5$ - Dam Location, $\theta_s = 140^0$	- Clearance = 0.102 mm (4 mil) - Pivot offset = 0.60 - Preload = 0 - Number of pads and arc length = $4/72^0$

IV. Solidworks models

Solidworks model of bearings

Constructing the bearings and housing started with using the Solidworks program.

Figure 6 shows the plain journal bearing 3D model. As you look at the bottom in the figure, there's a groove to limit the shaft from rotating the entire bearing. This feature is applied to all 3D printed bearings in this project.

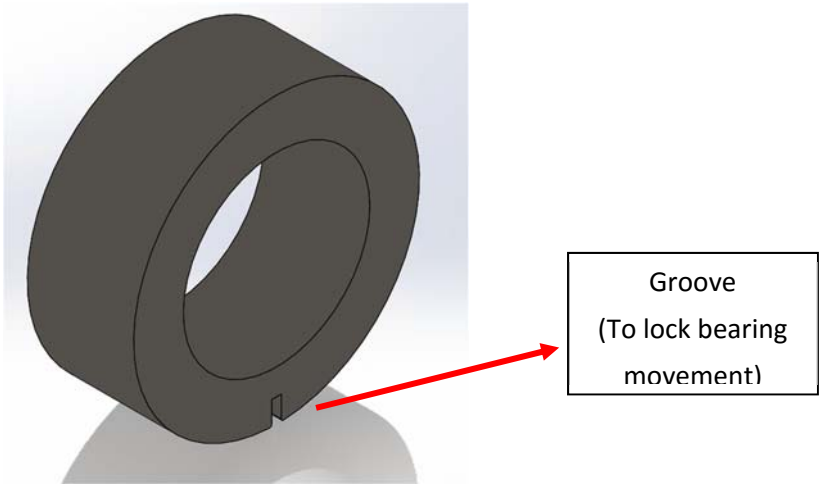

Figure 6 Plain Journal Bearing

Using similar geometry as the plain journal bearing, Figure 7 shows a pressure dam bearing model. Looking within the inner diameter there are grooves inside that cause the fluid to react similar to a Rayleigh step bearing configuration. Figure 8 gives a two dimensional view within the pressure dam bearing with the lubricant flowing from the right to the left.

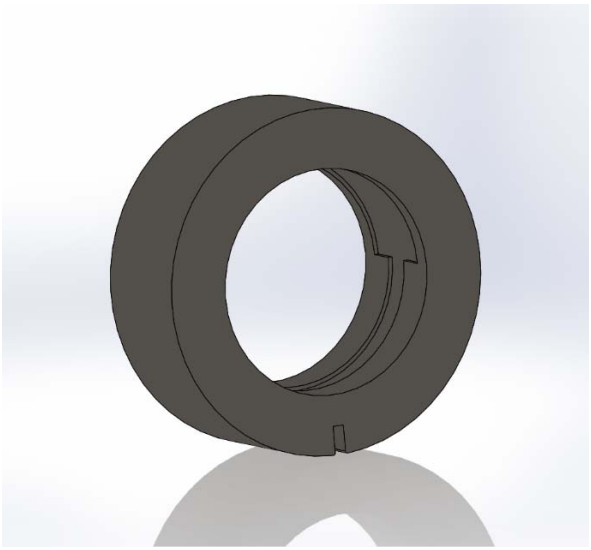

Figure 7 Pressure Dam Bearing Model

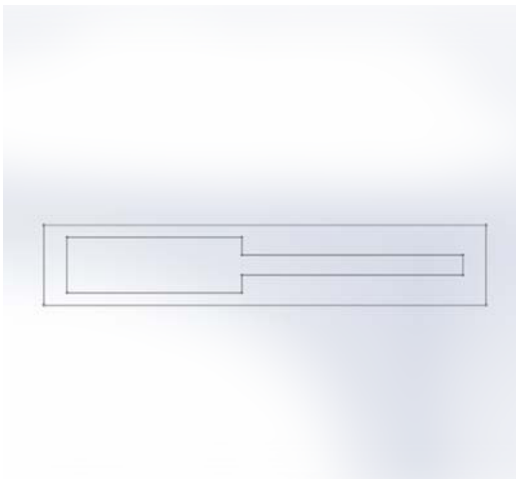

Figure 8 Pressure Dam Bearing Inner Diameter Layout

Flexure pivot bearing adds both the simplistic plain journal sketch and arduous complexity in pressure dam design. Simplistic as in the bearing doesn't need any extra features to remove material, as the pressure dam bearing needs cut revolve features. Complex as in the sketch will need to have a precise angle orientation for the tilting pads. This angle corresponds to pad offset, which is the ratio of distance between pad leading edge and minimum clearance to distance between leading and trailing edge. Figure 9 shows a sketch for the flex pivot pad. Figure 10 is the final model for the flex pivot bearing.

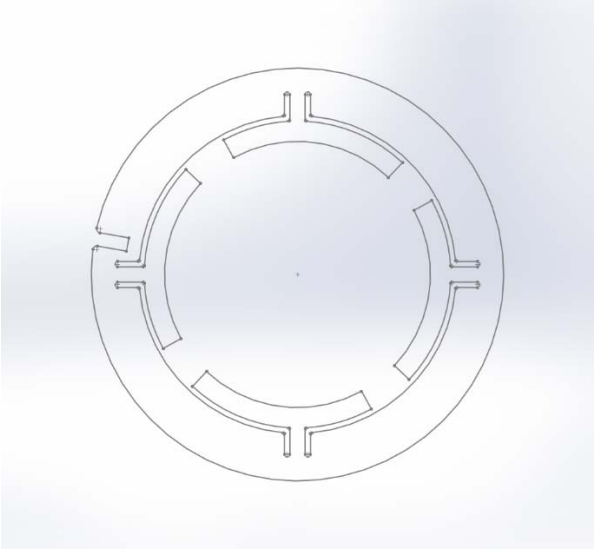

Figure 9 Flex Pivot Bearing Sketch

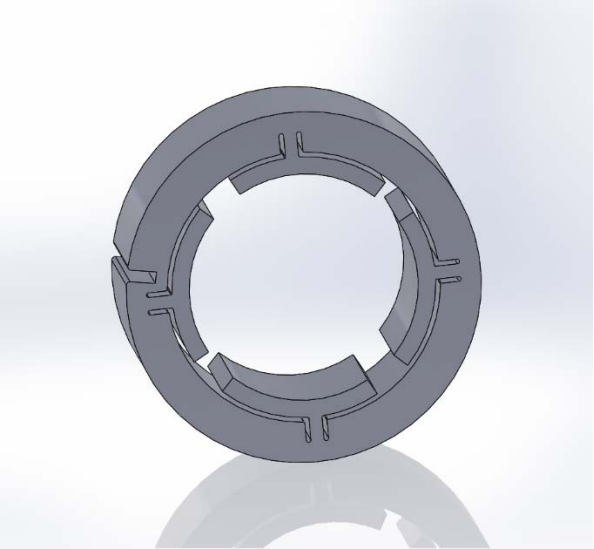

Figure 10 Flex Pivot Bearing Model

Solidworks model of bearing housing

The bearings go inside the housing that fits inside a cavity and are able to hold a load with an oil supply and rotor turning. Figure 11 shows the initial bearing housing that came with the Bentley Nevada kit. This housing has a permanent plain journal bearing within the housing itself. Several iterations or versions were modeled to follow this bearing housing.

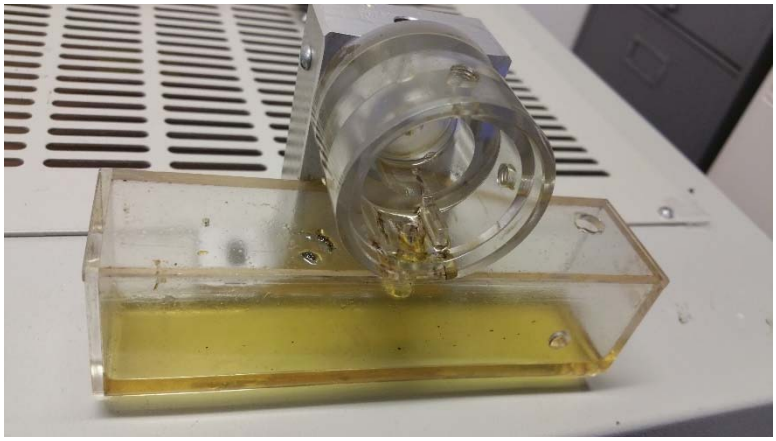

Figure 11 Initial Bearing housing

First issue when following this design involves accommodating space to insert custom bearing geometries. The center material is removed from within the housing. A lip is left to act as a key to not only make sure the bearings are inserted correctly but to also restrict the bearing from rotating when rotor is in motion. Figure 12 shows the model for the housing as it follows the housing design in Figure 11. To relieve stress in the bearing housing, filets were added on outside bearing housing to tank. The oil supply enters through the same location as the initial housing. It starts through the top of the back mount and exits at the center of bearing housing. Between the oil supply inlet and outlet there's a 90-degree bend with a large radius of curvature to accommodate for smooth flow for suppling oil. Several measurements were taken and adjusted for ease of access. Holes were added to place proximity probes. Figures below show the annotated drawing of the bearing housing.

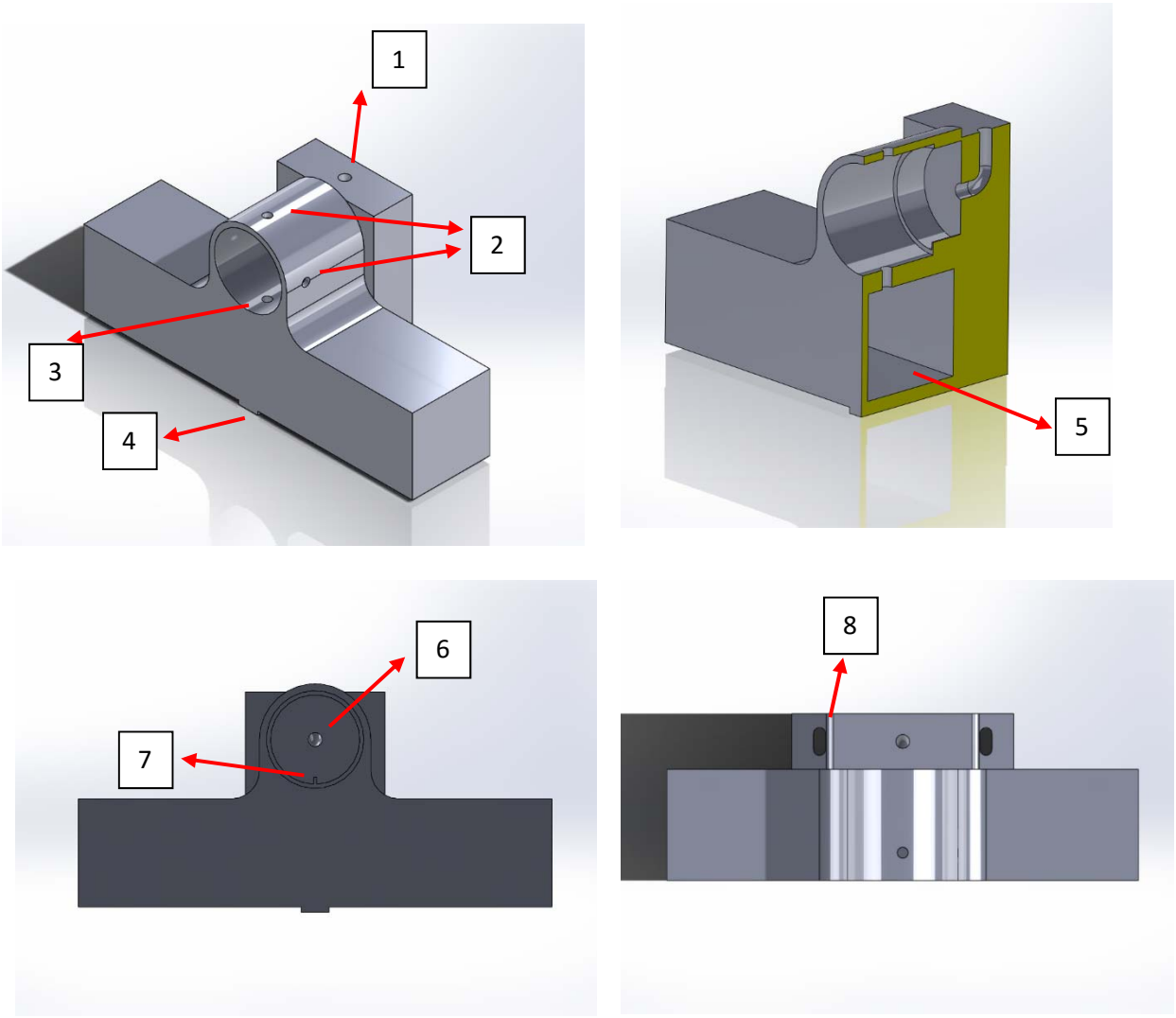

1. Oil inlet, draw oil from reservoir; 2. Holes for proximity probes; 3. Oil outlet to sump; 4. Groove to maintain orientation of housing. 5. Oil sump; 6. Oil outlet to bearing; 7. Lip for fitting the bearing 8. Holes to mount housing on the rotor kit

Figure 12 Annotated diagram of the bearing housing

V. 3D Printing Options

3D printing using Polyjet technique (High Fidelity)

Bearings modeled in solidworks were designed for 4 mil clearance. This calls for high fidelity printing, Table 4, located at Texas A&M University Mechanical Engineering using a process called Polyjet printing. This process incorporates depositing tiny photo-polymeric material droplets and cures (hardened) using UV light [9]. This process is shown in Figure 13. Along with the primary material, support material is printed around the surface of the finished product. This imparts the finished product very smooth surface finish. Post processing with water jet removes support material from finished product.

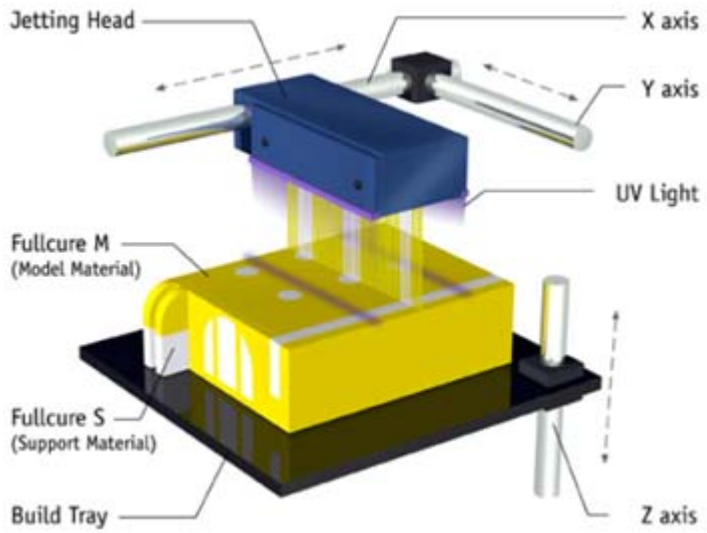

Figure 13 Polyjet printing technique [10]

Among the various high fidelity printers in the Texas A&M Mechanical Engineering 3D printing facility, Stratasys Connex 500 is the most precise 3D polyjet printer and on recommendation from 3D printing personnel. Most bearings in this project were printed on this printer. Print accuracy depends on various factors and typically, the final output shrinks due to cooling. Dimensions are generally smaller than the input dimensions. Several sophisticated software account for this shrinking factor, though it's not completely possible to eliminate dimensional error due to shrinkage. However, the 3D printing personnel guaranteed 80 microns (3 mil) accuracy (in the absence of multiple iterations) and the final output was expected to have an accuracy better than 3 mils.

An important point to note, is 3D printing process is repeatable. So, if a printed part is off by an accuracy of 1 mil, if it is reprinted with the same dimensions, it will still be off by 1 mil. In other words, 3D printing is precise but not accurate. Due to repeatability, a few iterations with solidworks dimensions can provide end user the desired accuracy, which for a Stratsys printer to could be as low as 0.3 mils. However, due to printing facilities time constraints and queue schedule for entire mechanical engineering department, performing multiple iterations proved impossible.

Table 4 Specification of high fidelity printer

Printer	Stratasys Connex 500
Printing process	Polyjet
Material	VeroWhite
Glass transition temperature (melting point)	54 ^{0}C
Expected accuracy (in the absence of multiple printing iterations)	80 microns (3 mils)
Precision	8 microns (0.3 mils)
Cost of material	$ 0.28/g
Cost of support material	$ 0.13/g

3D printing using Fused Deposition Modelling (Low Fidelity)

The bearing housing was printed using a Fused Deposition Modelling (FDM) printer, properties shown in Table 5. FDM is the most common form in 3D printing. This printing process consist heating thermoplastic amorphous material beyond its' glass transition temperature, where this converts from relatively brittle into a more ductile and viscous state. This viscous material is laid onto a plate layer by layer. The extrusion/heating process occurs at approximately 220-230 degrees Celsius and extrudes onto a plate. The plate temperature recorded at the 3D printing facility was around 60 degrees Celsius, which shows that the material cools down and hardens instantly. Figure 14 shows an example of FDM 3D printing. The accuracy of FDM process depends on various factors and typically, the final output shrinks due to cooling, similar to other printing methods.

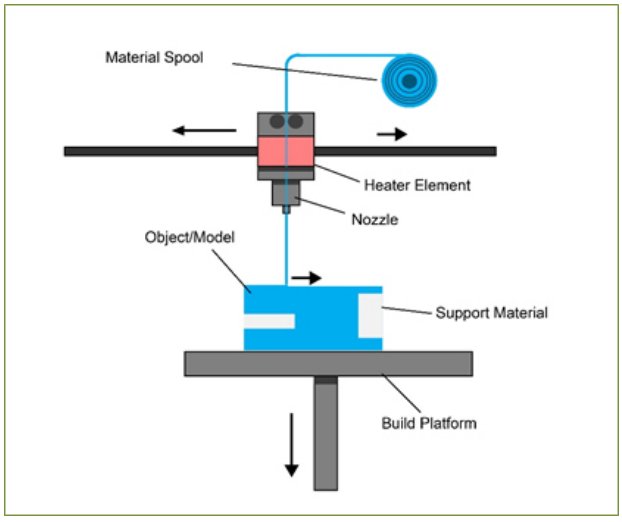

Figure 14 FDM printing technique [11]

FDM printers come with various accuracy specifications. A low fidelity FDM printer made the bearing housing using ABS plastic. The 3D printing facility personnel guaranteed a 500 microns (20 mils) while printing the bearing housing. A low fidelity printer was used because high accuracy was not required for

the bearing housing and also requires large print volume. Thus, cheaper material (ABS/PLA plastic) was used. After printing, the bearings fit nicely into the bearing housing and thus the choice of printer was justified. Table 5 shows the specifications of low fidelity printer.

Table 5 Specification of low fidelity printer

Printer	Low fidelity FDM printer
Printing process	FDM
Material	PLA plastic
Glass transition temperature (melting point)	55 ^{0}C
Expected accuracy (in the absence of multiple printing iterations)	250 microns (10 mils)
Precision	13 microns (0.5 mils)
Cost of material	$ 0.05/gram

VI. 3D print outputs

3D printed bearing housing

Once receiving the printed bearing housing, various modifications were made suitable for operation. These modifications can be seen in Figure 15 and have been properly annotated. It is important to note that 3D printing is done using routed layer material and inevitably this makes the finished product porous. Heating the external surface to above the melting point of the material can help seal the external surface. In this project, silicone was used in places where leaks were very substantial and is shown in Figure 15. Below are the modifications made in the bearing housing.

- Proximity probe holes were moved closer to the bearing (Annotation 1)
- Proper sealant was added in the hole connecting the reservoir to the housing to avoid leakage (Annotation 2)
- Holes in the sump give access to remove filler material from the cavity (Annotation 3)
- Hole was drilled in the sump to let oil flow out of it and avoid over flooding it (Annotation 4)
- Silicone was added to avoid leakage from various parts of the bearing housing (Annotation 5)

These modifications are labeled in the annotated diagram below.

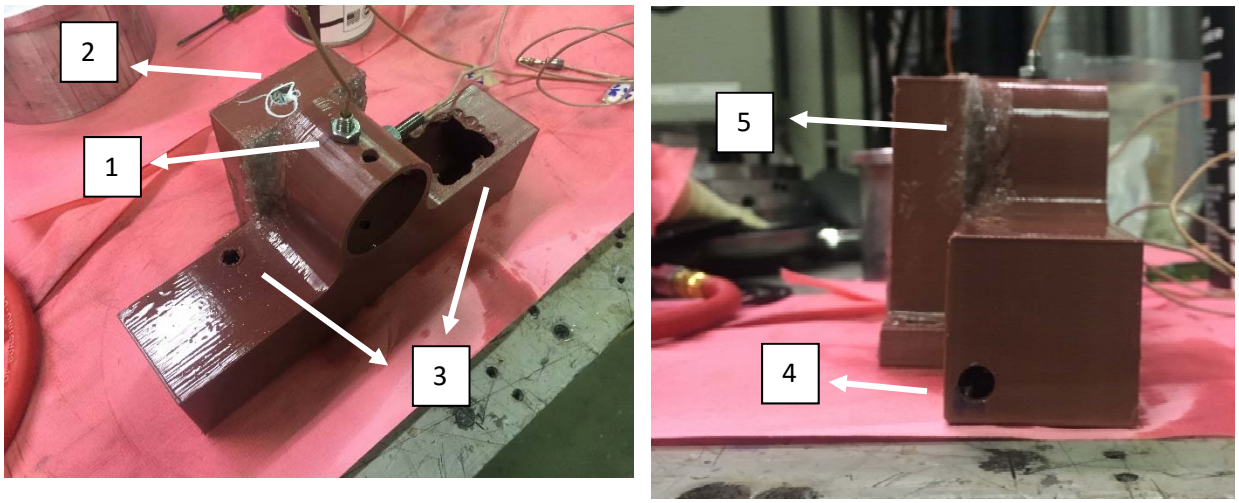

Figure 15 Annotated diagram of the 3D printed bearing housing

3D printed bearings

Four bearing were printed, three of them with Polyjet printing method and photopolymer material and one of them with FDM printing method and PLA material. The printed bearings are shown in Figure 16.

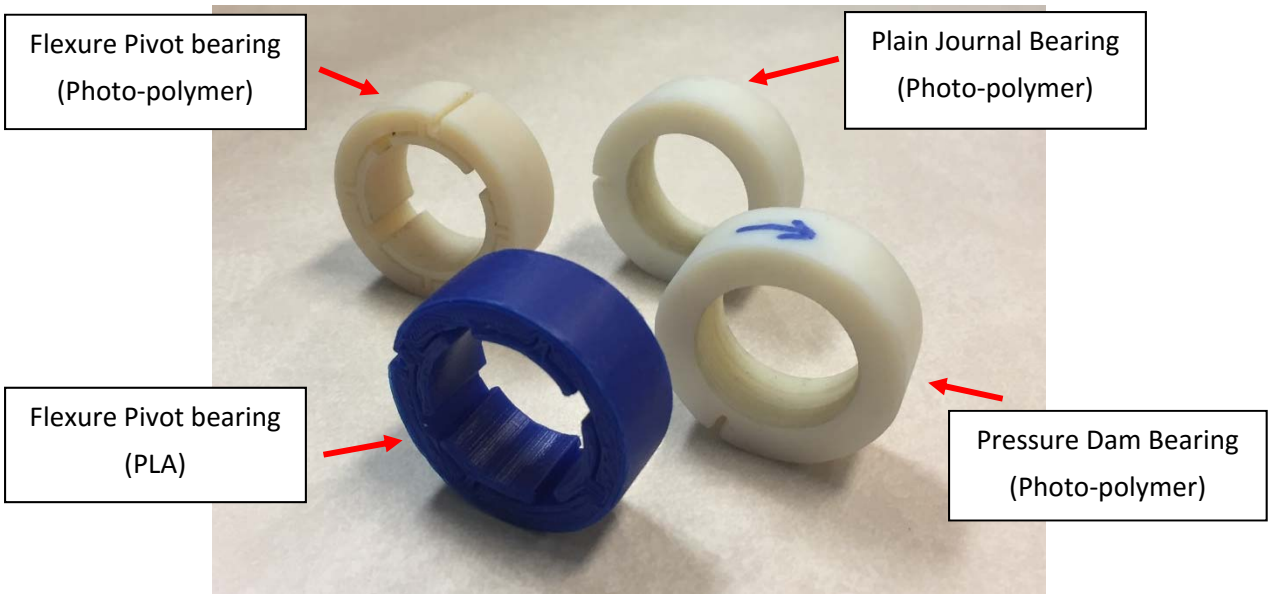

Figure 16 3D printed bearings

All the bearings were designed for a 4 mil radial clearance. However, due to shrinkage during printing, the final output had a different clearance and is tabulated below, Table 6.

Table 6 Final clearance of the bearings

	Material	Printing technique	Actual radial clearance
Flexure Pivot (PLA)	PLA	FDM	80 microns (3.2 mils)
Flexure Pivot (Photopolymer)	Photopolymer	Polyjet	76 microns (3.0 mils)
Plain Journal Bearing (Photopolymer)	Photopolymer	Polyjet	55 microns (2.2 mils)
Pressure Dam Bearing (Photopolymer)	Photopolymer	Polyjet	80 microns (3.2 mils)

VII. Experiment and Validation of Bearing Performance

Test setup description

The test setup after assembling the 3D printed parts and the sensors is shown in Figure 17. ISO VG 32 lubricant is used for testing (Refer to Appendix A for oil properties).

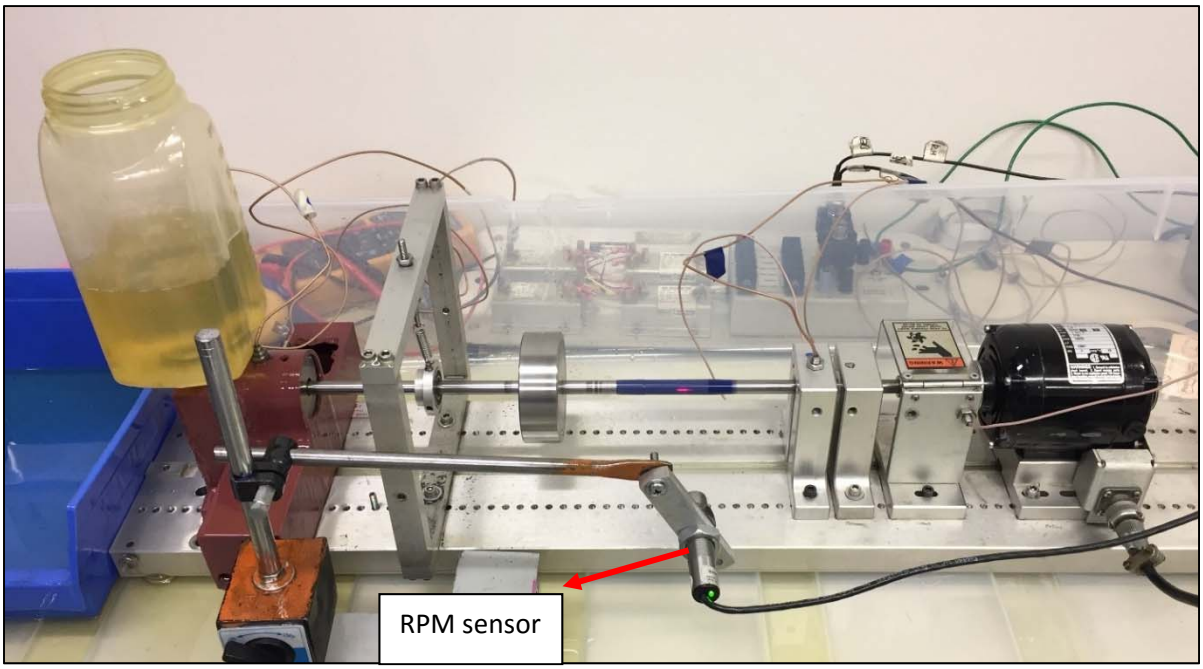

Figure 17 Final test setup

Table 7 shows the test matrix for the experiments.

Table 7 Test Matrix

	Bearing load			
	0N	**2N**	**4N**	**6.58N**
PLA flexure pivot bearing	[2000,5000,8000] rpm	[2000,5000,8000] rpm	[2000,5000,8000] rpm	[2000,5000,8000] rpm
Photopolymer flexure pivot bearing	[2000,5000,8000] rpm	[2000,5000,8000] rpm	[2000,5000,8000] rpm	[2000,5000,8000] rpm
Photopolymer plain journal bearing	[2000,5000,8000] rpm	[2000,5000,8000] rpm	[2000,5000,8000] rpm	[2000,5000,8000] rpm
Photopolymer pressure dam bearing	[2000,5000,8000] rpm	[2000,5000,8000] rpm	[2000,5000,8000] rpm	[2000,5000,8000] rpm

Measuring devices

Measuring devices used in this experiment are shown below.

Thermal Gun

Force meter

Voltmeter

Dial gauge

RPM sensor

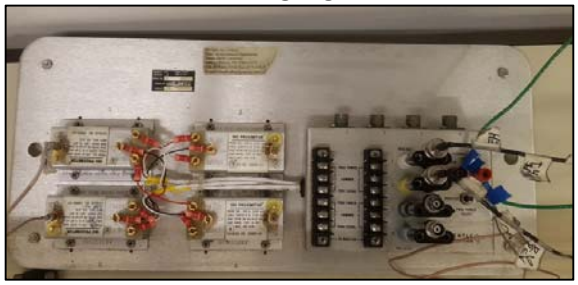

Proximity probe DAQ

Figure 18 Measuring devices

The precision of the measuring instruments are tabulated in Table 8.

Table 8: Precision of measuring instruments

Instrument	Uncertainty
FLUKE 561 Infrared Thermometer	± 1 % or ± 1 °C
AWS SR-20 Digital Hanging Scale	± 0.03 kg
Proximity Probe Channel-1	± 1.5x10^-5 mils
Proximity Probe Channel-2	± 9.1x10^-4 mils

Testing procedure

The proximity sensors, displacement probes, are set up and calibrated by using in-situ rotor. This importance in calibration insures sensors in use follow the scale factor specification, i.e. 200 mv/mil. One should bear in mind that the differing rotor material can affect the reading value of the probe. Thus, to avoid this uncertainty, the probe is calibrated follows the procedure below

Proximity probe calibration procedure

1. Set Voltage meter to measure output voltage from proximity probe output signal port
2. Record reference point at 0V, i.e. proximity probe attach to the shaft. One should note, higher gap distance between probe and rotor induces higher voltage output.
3. Gradually turn the probe away from rotor each 2V and record differing distance. This step is repeated until output voltage become 14V (maximum output from the panel is 15V).
4. Confirm linearity of the signal output and select proper gap/voltage to be installed for monitoring test. In this set up, the selected probes show good linear signal throughout the range from 2-14V. Thus, the gap voltage selected is 10V.

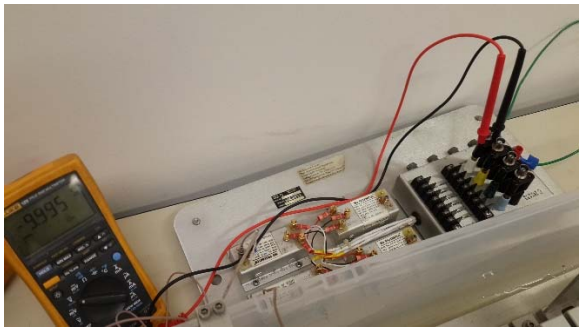

Figure 19 Setup of voltmeter

Figure 20 Checking travelling gap

The load in the experimental setup can be changed by adjusting the tightness in the spring attached to the ball bearing. For proper adjustment of the load, the following procedure is followed.

Load adjustment procedure

1. Loosen the spring support, let the rotor sit on the bearing
2. Use dial gauge to set rotor resting position, i.e. dial gauge reading is “A”

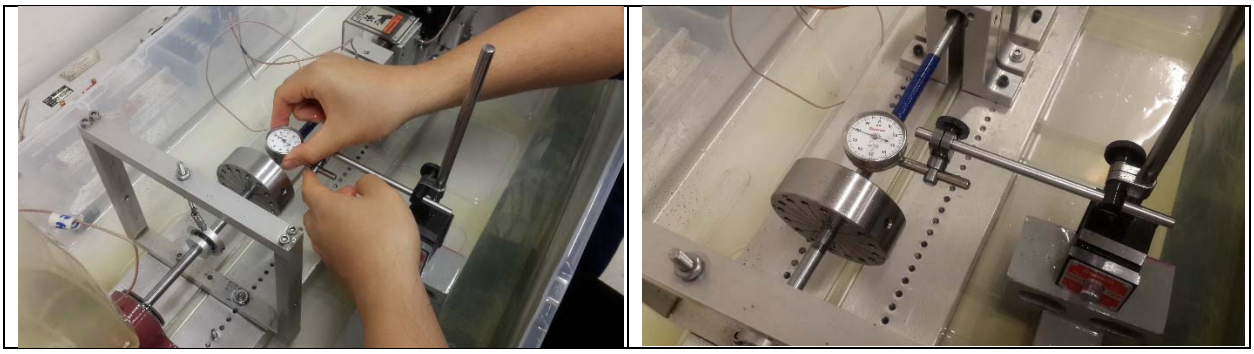

Figure 21 Setup of dial gauge

3. Remove bearing housing and use the spring hanger to support the rotor

Figure 22 Removal of bearing housing

4. Adjust spring length so the force meter mounted at the journal indicates the target loads, i.e. 0N, 2N, 4N, 6.58N. Restore and maintain the dial gauge reading ("A") when the force meter reaches the target.

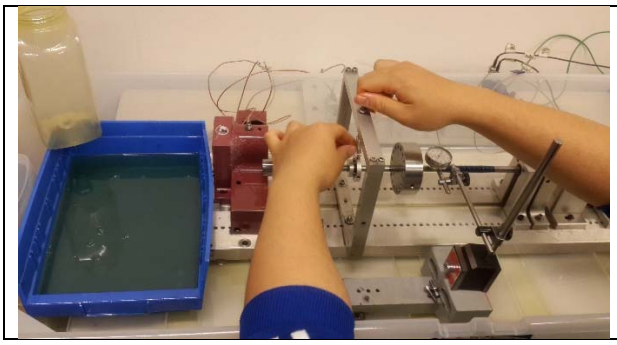

Figure 23 Adjusting spring to the required load

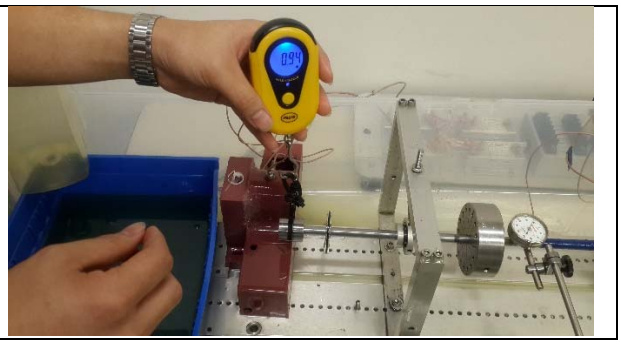

Figure 24 Confirming static load with hanging scale

5. Re-install the bearing housing. Make sure that the dial gauge reading is still "A".

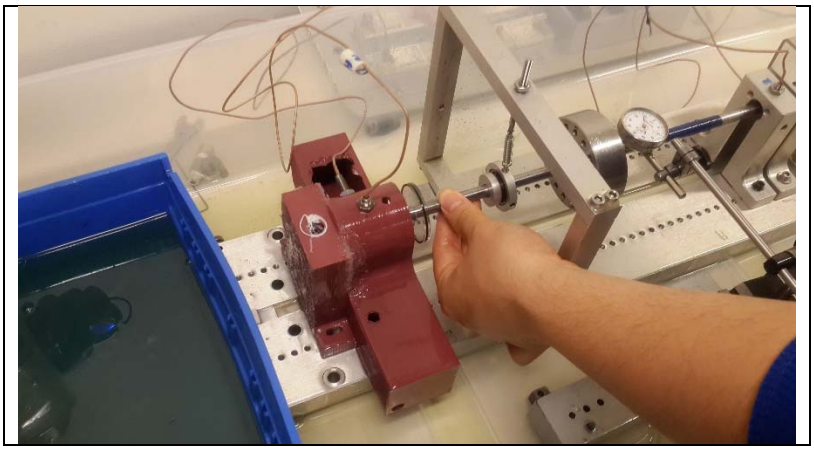

Figure 25 Confirming rotor position using dial gauge

Before beginning a test run, the proximity probes are connected to the data acquisition unit and this data is recorded on the ADRE software present in the PC. It should be noted that data from only the non-drive end proximity probes were collected. The motor and the RPM sensor are connected to the power source.

Description of each test run

Each test run was completed using the following set of test procedures:

- The RPM of the motor is ramped up to 2000 RPM and held constant at that RPM for some time.
- The time taken to drop the oil level in the reservoir from 16 ounces to 12 ounces is recorded. This provides an estimate of the flowrate.
- Using a thermal gun temperature at the inlet and at the outlet is measured. Temperature measurements are taken after a while, so that temperature stabilizes at a constant value. Bearing vibration is also recorded using ADRE system.
- The RPM is ramped up to 5000 RPM and the same procedure is repeated. The same procedure is again repeated for 8000 RPM.

VIII. Results and Discussion

Static Predictions and Results

The bearing code XL_JB_PRESS_DAM™ was used to predict the steady state solution of the plain journal bearing, and pressure dam bearing. For the PJB the measured flow rate is higher than predicted for all cases, see Figure 26. The predictions follow the same trend as the measured results, flow increases with speed and load. Predicted temperature rise in the PJB was much higher than measured, see Figure 27. The trend of the predicted values is the same as the measured results, temperature rise increases with speed and decreases with load. The under prediction of the flow rate may explain the over prediction of the temperature rise. As flow increases, temperature rise decreases as more energy is pulled away by the lubricant.

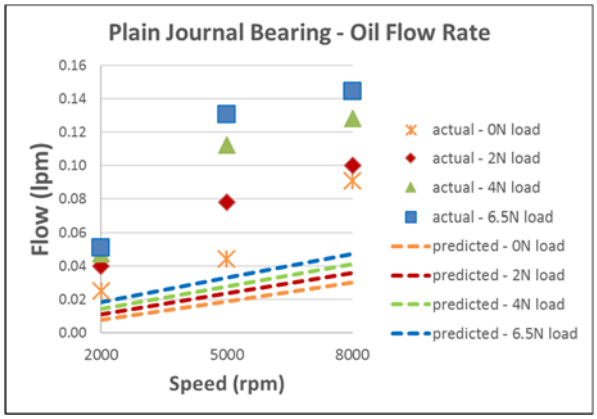

Figure 26 Plain journal bearing measured and predicted oil flow rates

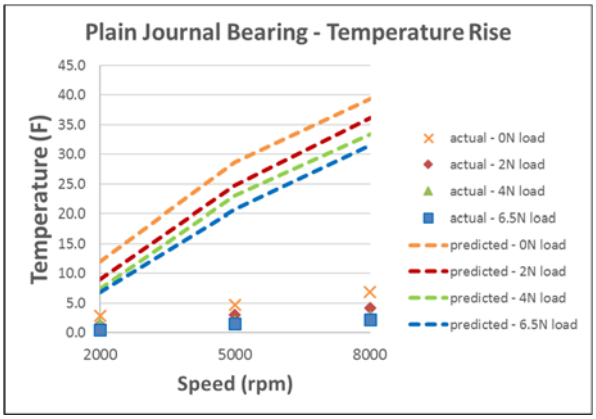

Figure 27 Plain journal bearing measured and predicted temperature rise

Predicted flow rates in the pressure dam bearing is higher than what was measured for all test conditions, see Figure 28. Flow rate increases with speed for both predicted and measured values, however, the predicted values do not significantly change with load. As seen in Figure 29, the predicted temperature rise is reasonably close to measured values. Temperature rise for predicted and measured values both increase with speed, however, predicted values are not dependent on load.

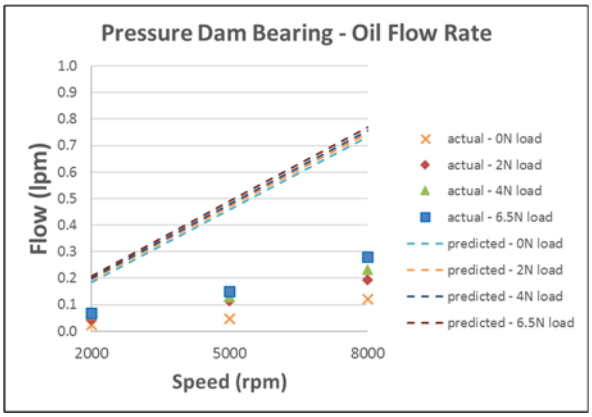

Figure 28 Pressure dam bearing measured and predicted oil flow rates

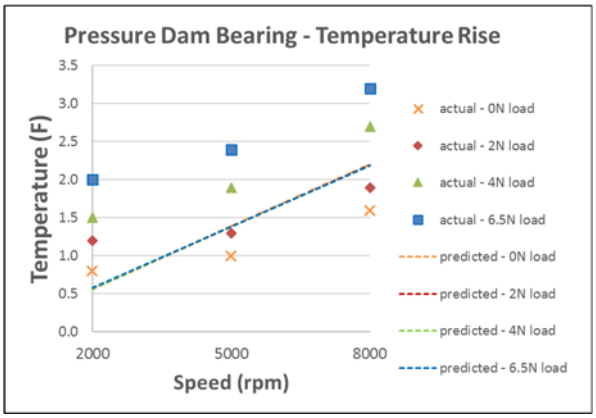

Figure 29 Pressure dam bearing measured and predicted temperature rise

Eccentricity of the rotor was predicted for all bearings and follow an expected trend in increasing eccentricity with decreasing Sommerfeld number. Unfortunately, measured rotor eccentricity values were not believable and could not be compared to the predicted values.

The flexure pivot bearing was tested without an end seal, as a result, a significant portion of the lubricant was able to leak between the pads. Predicted values are not expected to be consistent with the measured values and no comparison can be made.

Dynamic Results

Table 9 presents a summary of the four bearings' performance, including: PLA flexure pivot, photopolymer flexure pivot, photopolymer plain journal, and photopolymer pressure dam bearings. Each bearing performance is evaluated at three different speeds, such as 2000, 5000, and 8000 rpm, and four different loads, i.e. 0, 2, 4, and 6.58N. The performance is examined using bode plots and cascade plots extracted from an ADRE system. Bode plots provide an overall view of bearing vibration at different running speeds and system critical speed, while cascade plots give an idea about system instability, i.e. sign of subsynchronous vibration.

Table 9: Summary of bearing performance

		Vibration amplitude (mils pk-pk)			Critical speed	Sign of instability
	Load (N)	@2000 rpm	@5000 rpm	@8000 rpm		
Flexure pivot (PLA)	**0**	0.75	2.5	2.75	4.5mils @2400rpm	yes. Start @5000rpm
	2	1	2.5	2.5	5mils @2400rpm	no
	4	1	1.5	2	5mils @2400rpm	no
	6.58	1	2	2	5mils @2400rpm	no
Flexure pivot (photopolymer)	**0**	2	4	4	split: 3mils @2000rpm & 3.75mils @2500rpm	yes. Start @5000rpm
	2	1	1.5	3	split: 1.25mils @1850rpm & 2.5mils @2400rpm	yes. Start @8000rpm
	4	0.75	1.5	2	split: 1.25mils @1900rpm & 1.5mils @2400rpm	no
	6.58	1	2	2.5	3.5mils @2500rpm	no
Plain journal (photopolymer)	**0**	3	2	2.25	7mils @2400rpm	no
	2	2	2	2	5mils @2400rpm	no
	4	1.5	2	2	6mils @2400rpm	no
	6.5	1	1.5	1.5	5mils @2400rpm	no
Pressure dam (photopolymer)	**0**	0.75	1.75	1.5	5mils @2350rpm	no
	2	0.5	1.75	2	6mils @2400rpm	no
	4	0.75	1.5	1.5	5.5mils @2400rpm	no
	6.58	1	1.75	1.75	5mils @2400rpm	no

The discussion compares performance of flexure pivot with 2 different materials (i.e. photopolymer vs PLA) and 3 different bearing design, all made from photopolymer (i.e. flexure pivot, plain journal, and pressure dam bearings).

Figure 30 to Figure 37 show bode plots, while Figure 38 to Figure 45 show cascade plots for flexure pivot bearings with different loads and materials.

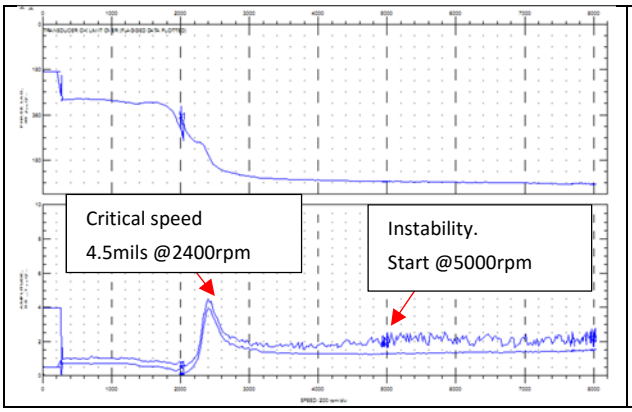

Figure 30: PLA Flexure pivot bearing - Bode plot at 0N load

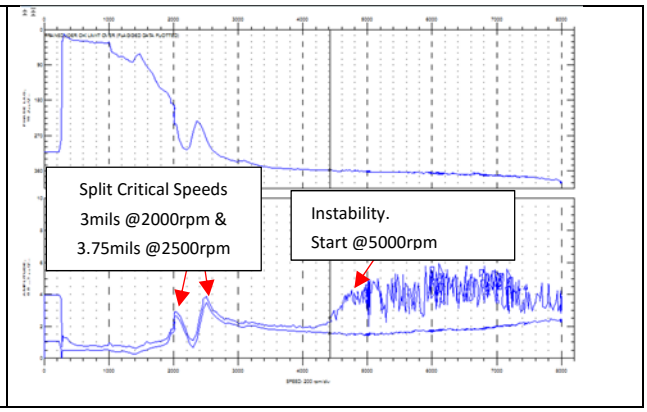

Figure 31: Photopolymer flexure pivot bearing - Bode plot at 0N load

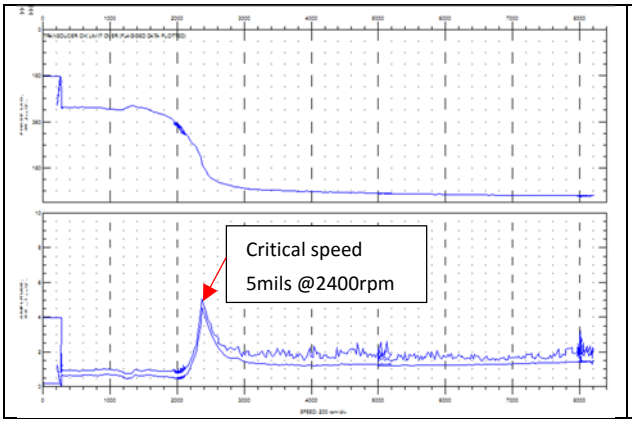

Figure 32: PLA Flexure pivot bearing - Bode plot at 2N load

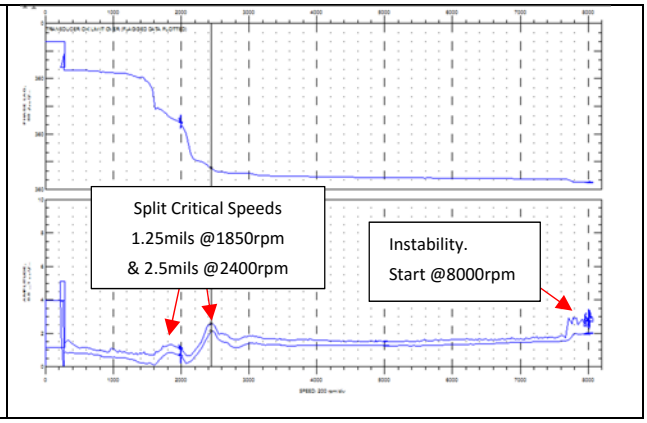

Figure 33: Photopolymer flexure pivot bearing - Bode plot at 2N load

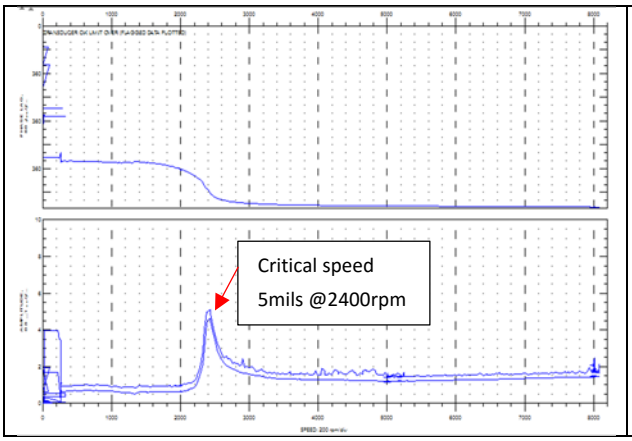

Figure 34: PLA Flexure pivot bearing - Bode plot at 4N load

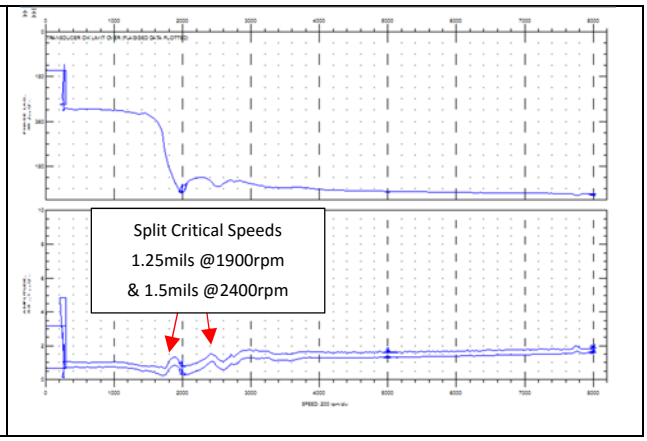

Figure 35: Photopolymer flexure pivot bearing - Bode plot at 4N load

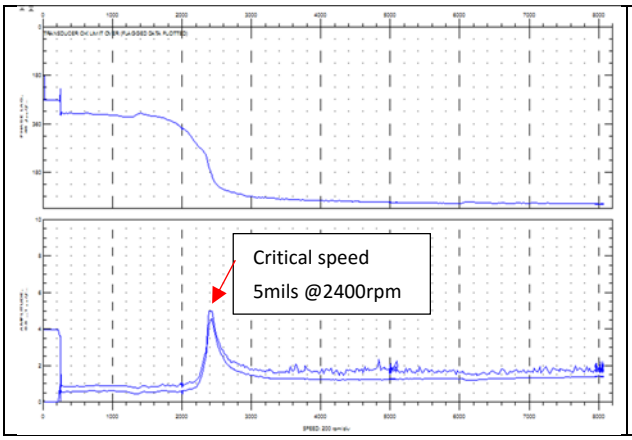

Figure 36: PLA Flexure pivot bearing - Bode plot at 6.58N load

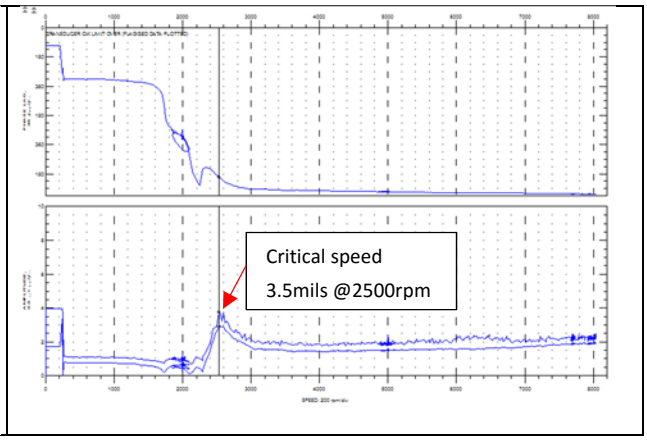

Figure 37: Photopolymer flexure pivot bearing - Bode plot at 6.58N load

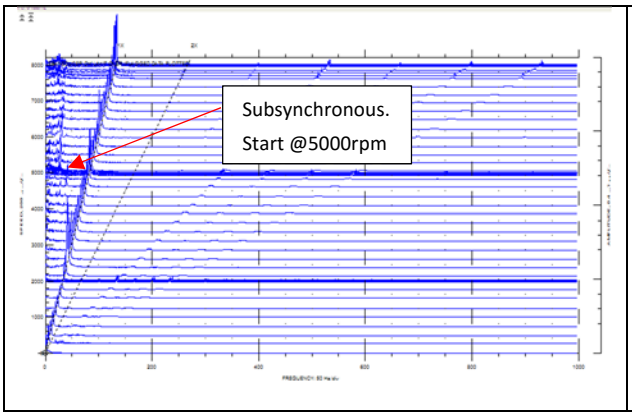

Figure 38: PLA Flexure pivot bearing - Cascade plot at 0N load

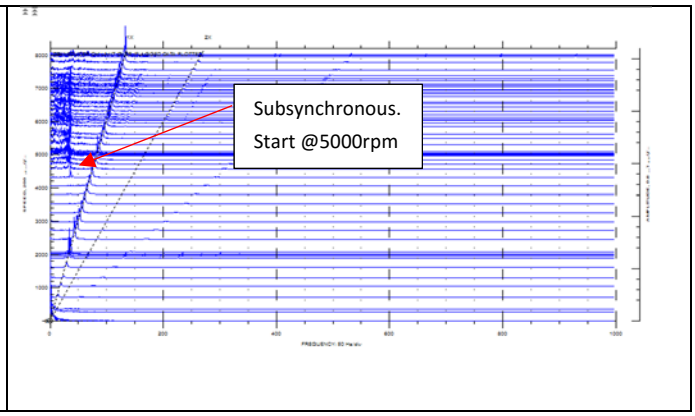

Figure 39: Photopolymer flexure pivot bearing - Cascade plot at 0N load

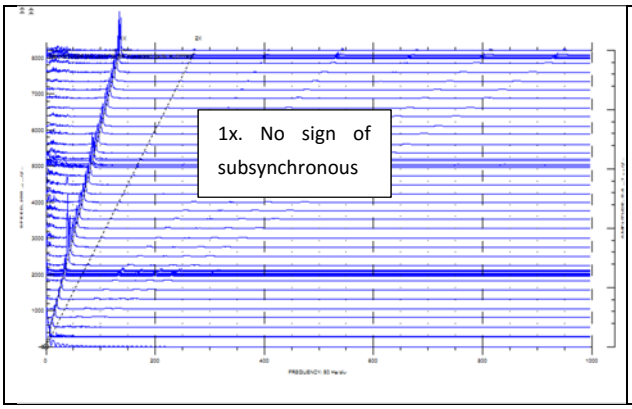

Figure 40: PLA Flexure pivot bearing - Cascade plot at 2N load

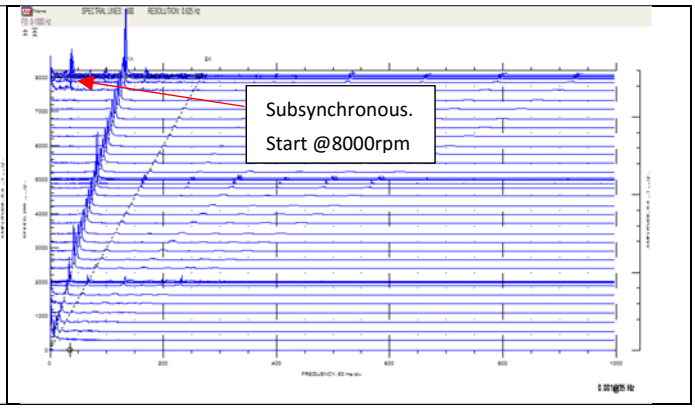

Figure 41: Photopolymer flexure pivot bearing - Cascade plot at 2N load

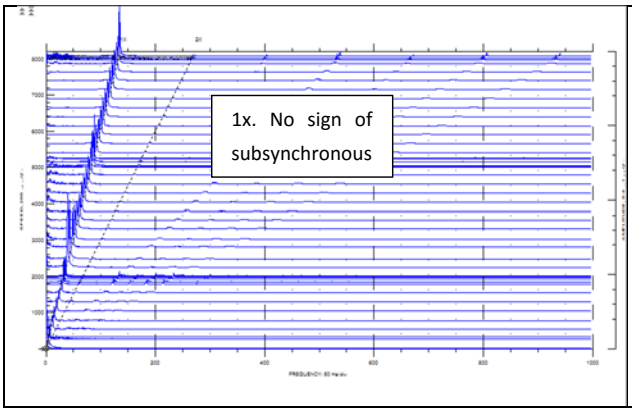

Figure 42: PLA Flexure pivot bearing - Cascade plot at 4N load

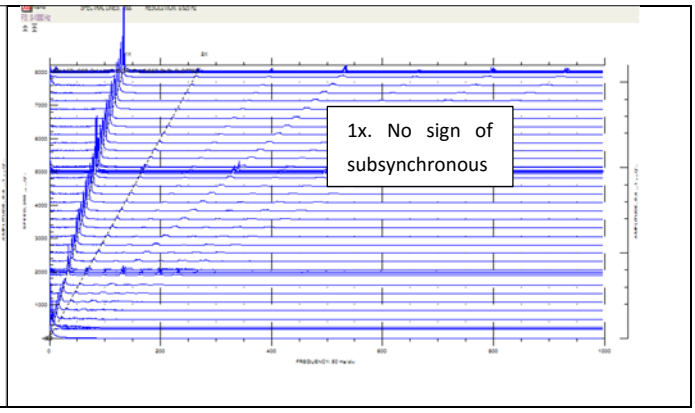

Figure 43: Photopolymer flexure pivot bearing - Cascade plot at 4N load

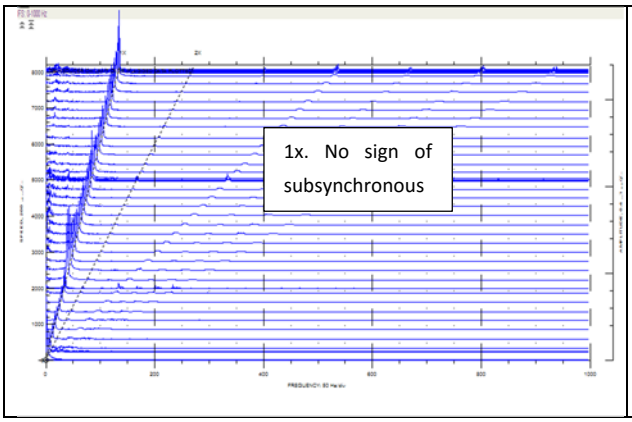

Figure 44: PLA Flexure pivot bearing - Cascade plot at 6.58N load

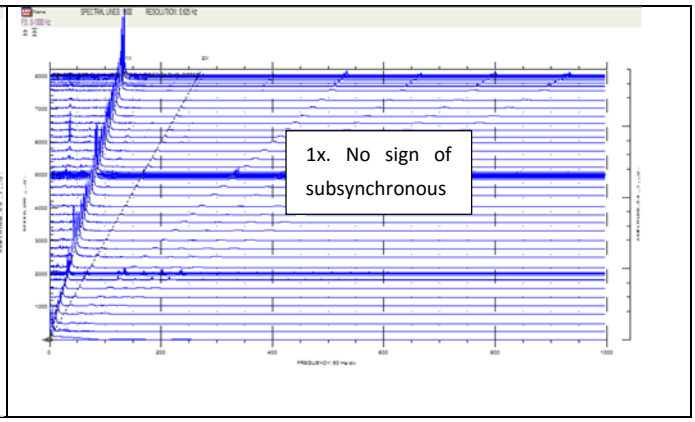

Figure 45: Photopolymer flexure pivot bearing - Cascade plot at 6.58N load

For photopolymer flexure pivot bearing, as shown in Figure 31, Figure 33 and Figure 35, there is evidence showing split critical speeds, i.e. due to orthotropic characteristic of the bearing. This is not observed in PLA material, shown in Figure 30, Figure 32, and Figure 34, even though both bearings have same physical dimensions. PLA material has an elasticity modulus at about 3.5GPa, while photopolymer material's elasticity modulus is ranging from 3.2-3.5GPa. In this study, material elasticity seems to have an effect on bearing stiffness in XX and YY directions, similar to a test result presented in [12] for tilting pad journal bearing. The existing of split critical speed brings down vibration amplitude at critical speed, i.e. 4.5mils for single critical speed of PLA bearing vs. 3.75mils max for split critical speed of photopolymer bearing. Generally, the photopolymer flexure pivot bearing provides a better response at the critical speed than the PLA flexure pivot bearing.

On the other hand, on an unloaded condition, i.e. 0N load, when the rotor speed reaches to 5000rpm, both PLA and photopolymer flexure pivot bearing show a sign of instability (Figure 30 and Figure 31). Figure 38 and Figure 39 shows sub-synchronous vibration at natural frequency when the speed is above 5000rpm as well. This normally does not happen in tilting pad or flexure pivot bearing, but it is reasonable to observe when the load is very low. When the load is increased to 2N, instability is eliminated on PLA

flexure pivot operation (Figure 40) but it still exists on photopolymer one when the speed is about 8000 rpm (Figure 41). An increment of load helps to move the journal center during operation which reduces chance of instability. It is obvious when no instability is observed at running loads of 4N and 6.58N for both bearings (Figure 42 to Figure 45). Using photopolymer increases a chance of instability when running at high speed and low load condition.

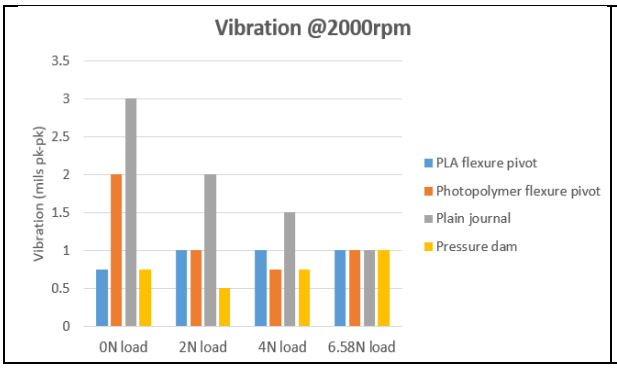

Figure 46: Bearing vibration comparison at 2000rpm

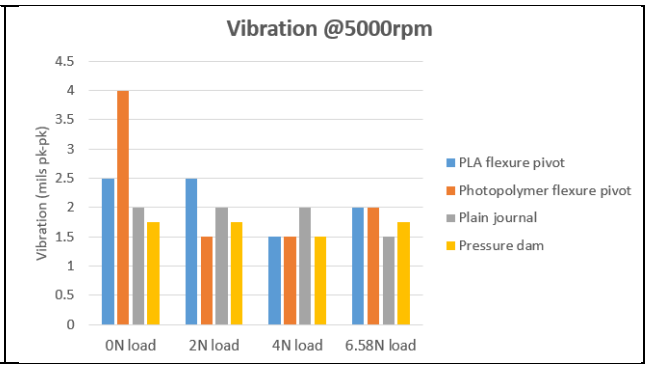

Figure 47: Bearing vibration comparison at 5000rpm

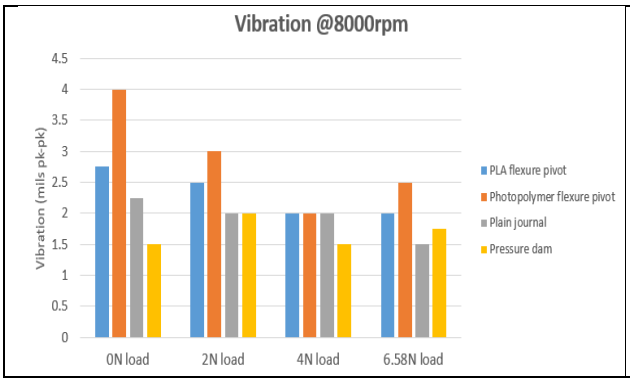

Figure 48: Bearing vibration comparison at 8000rpm

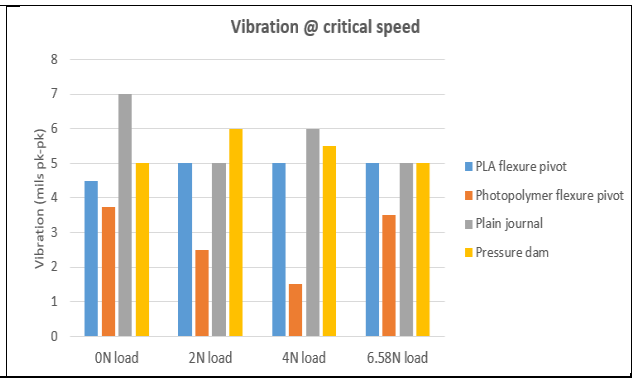

Figure 49: Bearing vibration comparison at critical speed

As shown in Figure 46 to Figure 48, the PLA flexure pivot bearing overall provides a better performance at running speeds of 2000, 5000 and 8000 rpm than the photopolymer flexure pivot bearing. However, at during operation at critical speed, photopolymer flexure pivot bearing gives a lower vibration than PLA flexure pivot bearing (Figure 49) due to existence of split critical speed and an orthotropic bearing characteristic.

Another interesting point from Figure 49, vibration of flexure pivot at critical speed is load dependent while the rest of bearings are load independent.

Similarly, Figure 50 to Figure 57 show bode plots, while Figure 58 to Figure 65 show cascade plots for flexure pivot bearings with different loads and materials. As shown in Figure 58 to Figure 65, there is no sign of instability for both journal and pressure dam bearings operating from 0N to 6.58N load.

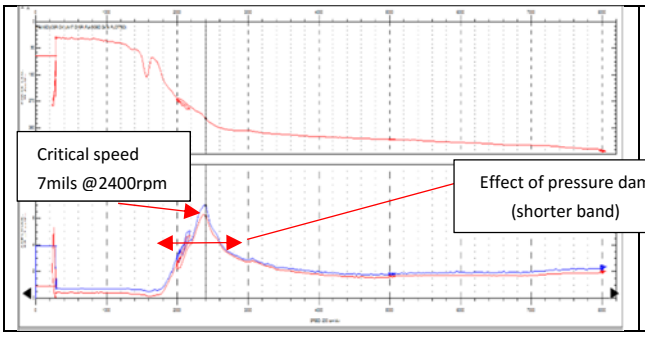

Figure 50: Plain journal bearing - Bode plot at 0N load

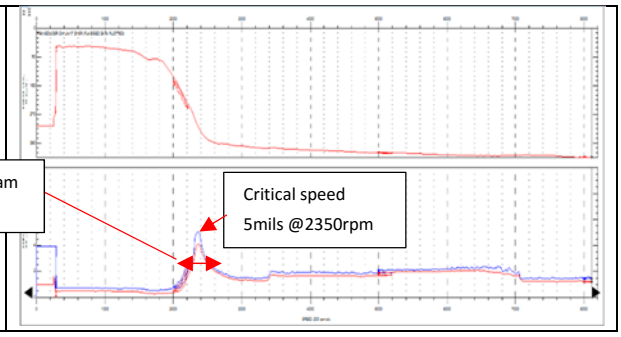

Figure 51: Pressure dam bearing - Bode plot at 0N load

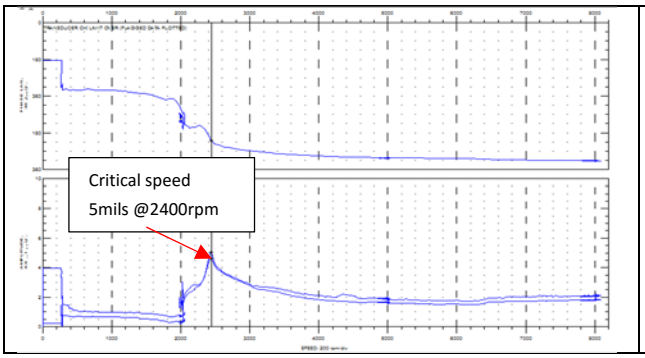

Figure 52: Plain journal bearing - Bode plot at 2N load

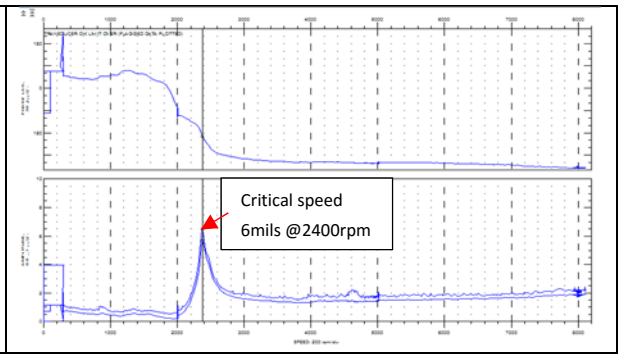

Figure 53: Pressure dam bearing - Bode plot at 2N load

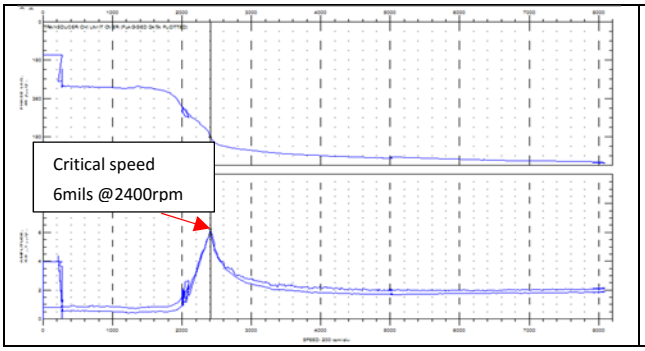

Figure 54: Plain journal bearing - Bode plot at 4N load

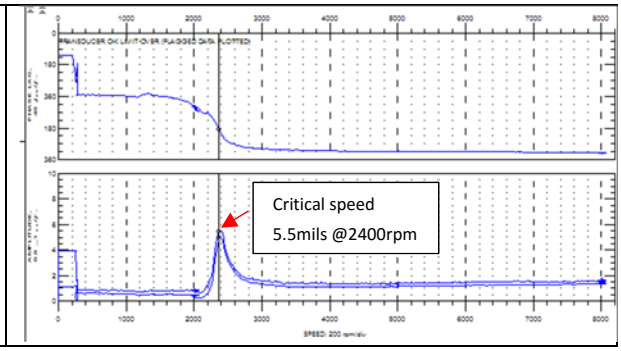

Figure 55: Pressure dam bearing - Bode plot at 4N load

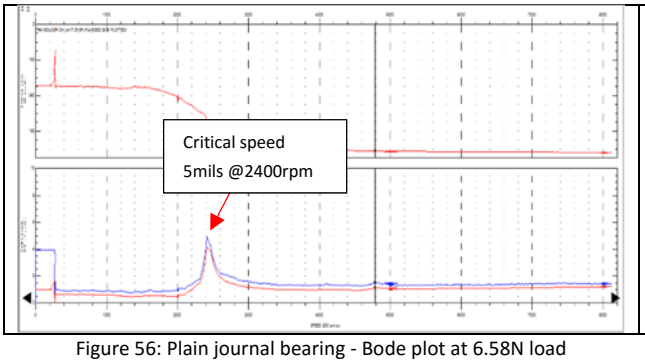

Figure 56: Plain journal bearing - Bode plot at 6.58N load

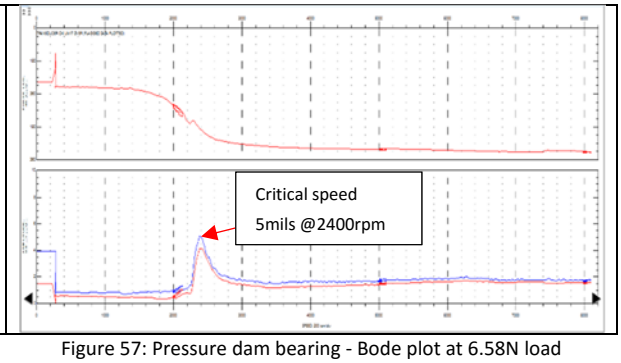

Figure 57: Pressure dam bearing - Bode plot at 6.58N load

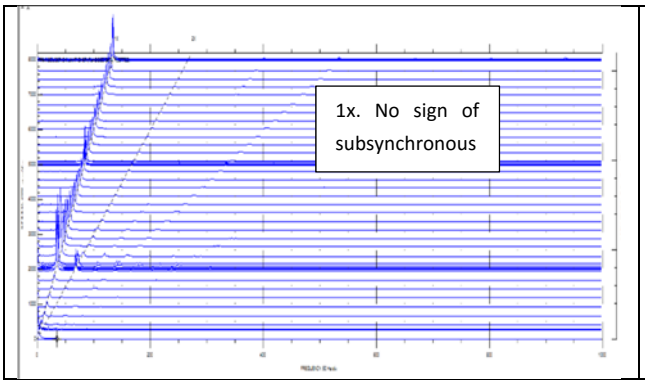

Figure 58: Plain journal bearing - Cascade plot at 0N load

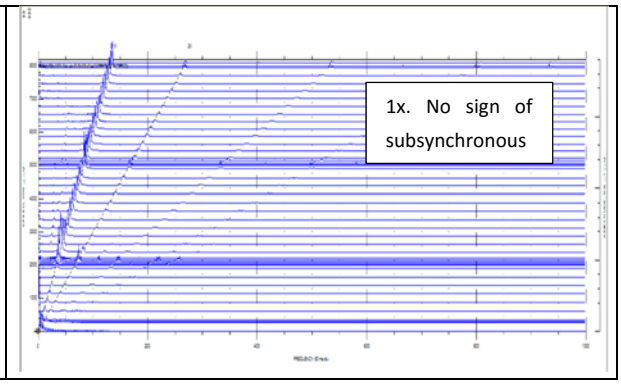

Figure 59: Pressure dam bearing - Cascade plot at 0N load

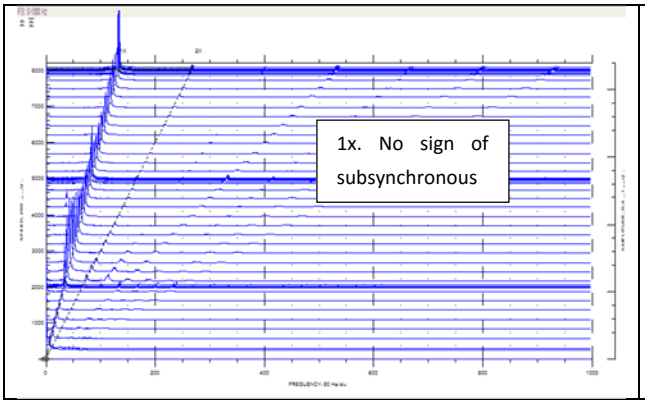

Figure 60: Plain journal bearing - Cascade plot at 2N load

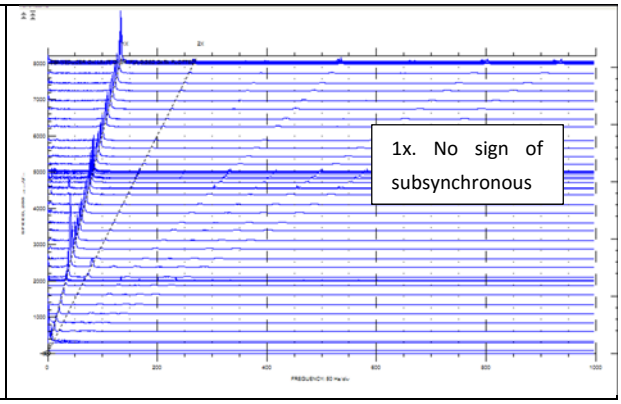

Figure 61: Pressure dam bearing - Cascade plot at 2N load

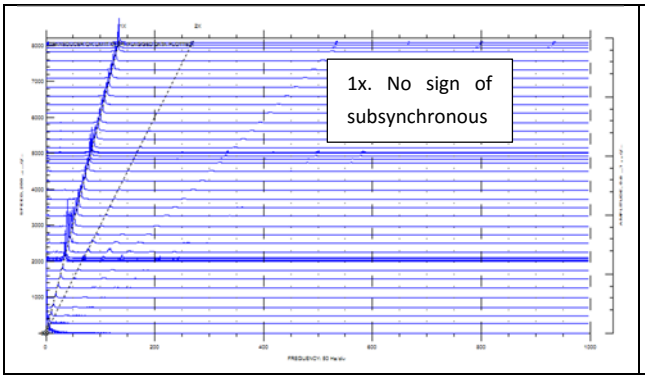

Figure 62: Plain journal bearing - Cascade plot at 4N load

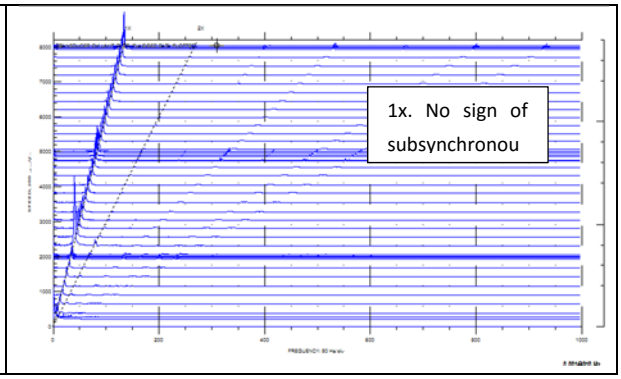

Figure 63: Pressure dam bearing - Cascade plot at 4N load

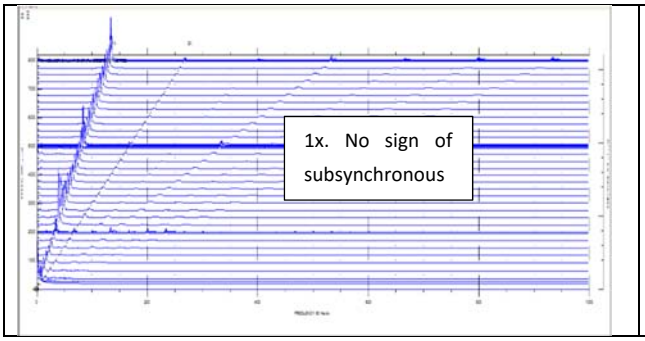

Figure 64: Plain journal bearing - Cascade plot at 6.5N load

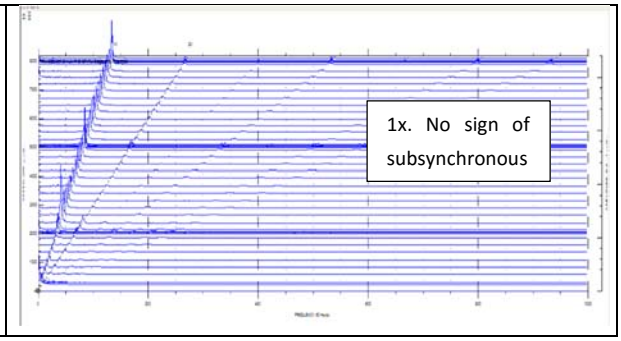

Figure 65: Pressure dam bearing - Cascade plot at 6.5N load

A narrow speed range of vibration response at critical speed region reflects the effect of pressure dam design. For an example, comparing vibration response of the journal bearing and pressure dam bearing operating at critical speed for 0N load, shown in Figure 50 and Figure 51. The pressure dam bearing gives a shorter speed bandwidth operating at critical speed than the journal bearing does. This character is quantified in parameter term Synchronous Amplitude Factor [13]. With higher Sync Amp Factor, damping lowers. Similarly, the effect of damping is also observed in Figure 52 to Figure 57 for the other bearing loads. With an effect of damping, the bearing vibration of a pressure damp bearing at 2000 rpm, which is nearly the critical speed at 2400 rpm, is much lower than the vibration of a journal bearing, data comparison shown in Figure 46.

Figure 66 and Figure 67 show the effect of pressure dam on the shaft orbit at the critical speed. Pressure damp helps to dampen the orbit size in vertical direction.

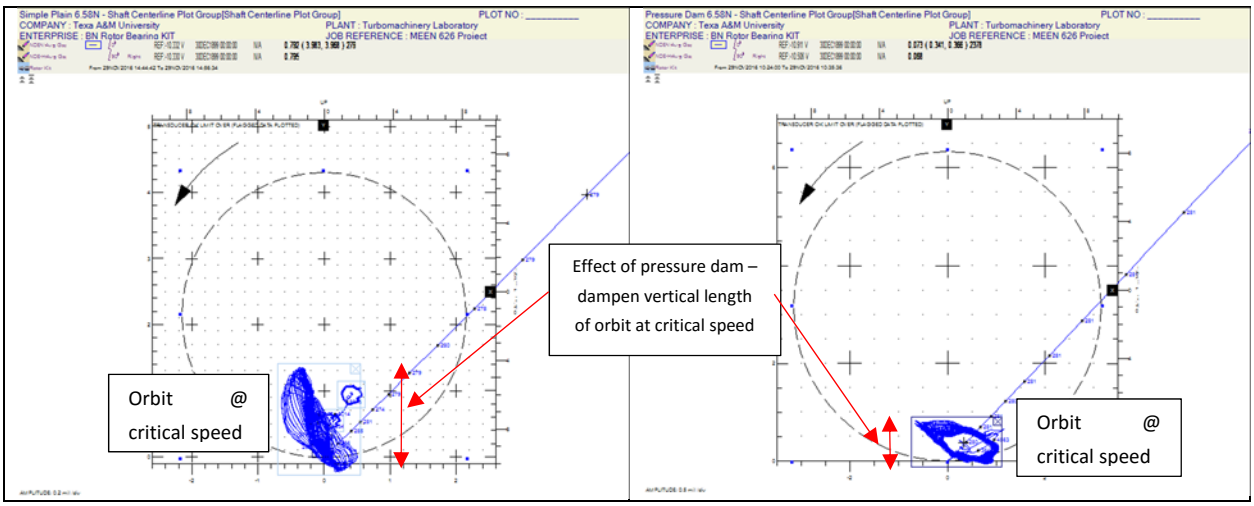

Figure 66: Centerline plot for the plain journal bearing operating at 6.58N load

Figure 67: Centerline plot for the pressure dam bearing operating at 6.58N load

To sum up, as shown in Figure 46 to Figure 49,

- Pressure dam bearing provides the best performance in term of vibration at 2000, 5000, and 8000 rpm among the 4 bearings.
- @2000rpm, the journal bearing operates poorly while at above 5000rpm, photopolymer flexure pivot bearing experience instability for low load operating condition.
- Due to an effect of split critical speeds, photopolymer flexure pivot bearing brings down the max vibration at critical speed while pressure damp bearing helps to narrow down the speed band at critical speed condition

IX. Recommendations

- Noticing the shortcomings of the bearing housing, a modified bearing housing was designed. Future students could take benefit of this re-designed bearing housing. Figure 68 shows the design of the new bearing housing.

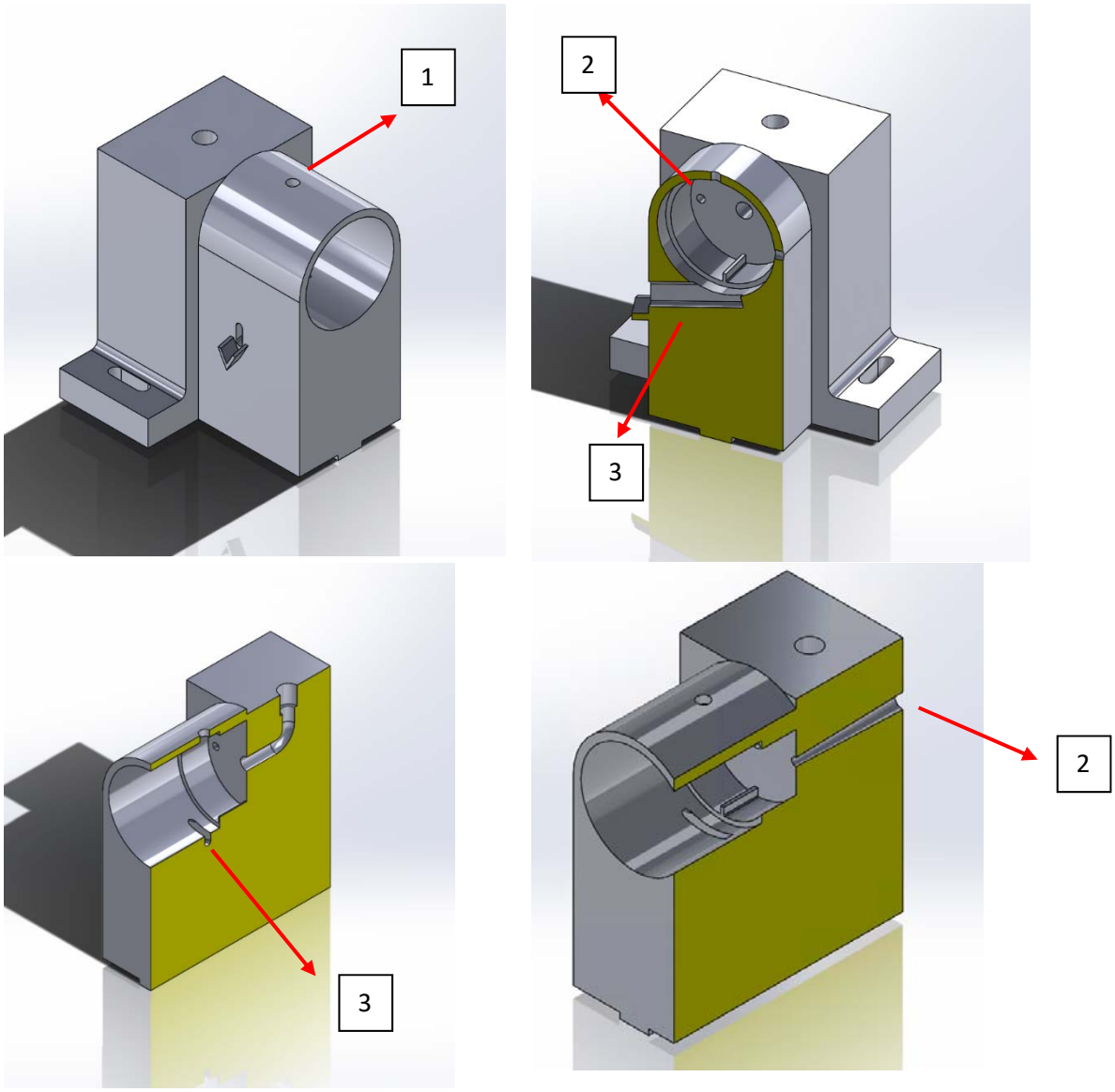

1. Proximity probe holes moved closer to bearing; 2. Added holes for easy removal of bearing; 3. New passage for oil out

Figure 68 Annotated diagram of new bearing housing

- 3D printing is precise but not accurate. Therefore, students are advised to perform multiple iterations until the desired accuracy is obtained.
- The measured eccentricity values were not reasonable. Some of the possible causes of this could be:

- There was no proper fit between the bearing housing and the bearings due to plastic shrinkage during printing. This can be addressed by performing multiple iterations of print until desired accuracy is obtained.
- Clearance likely change before, during and after the test. This might affect the measured eccentricities. Several measurements of clearance before and after the test should be done.
- Unavoidable human error during load adjustment procedure.

X. Future Work

- The test matrix needs to be expanded to check the effect of different material (PLA, ABS, Photo-polymer) on the performance of bearings. The difference of material will be most pronounced in Flexure Pivot Bearings, since different materials have different modulus of elasticity.
- Surface roughness needs to be documented and the effect of surface roughness needs to be studied. Surface roughness can be varied by using different types of sand papers/filers.
- Experiments show that 3D printed materials are porous. The effect of porosity needs to studied. Porosity can be varied using different 3D printing techniques and by choosing the fineness of the print in the 3D printing software.

XI. Conclusion

With advances in additive technology, 3D printing provides an alternative manufacturing methods with many benefits. Inline to this modern method, this study compares experimental and numerical results of various 3D printed bearing designs. To achieve this objective, Bentley Nevada rotor kit provides experimental results, which are then compared with predications obtained from XLTRC^2 software.

For this study, three different bearing designs were considered: Plain Journal, Pressure Dam and Flexure Pivot bearing. Through literature review, optimum bearing dimensions are obtained and modelled into Solidworks. There are two printing techniques i.e. Polyjet (which used photopolymer) and Fused Deposition Modelling (which uses PLA) used for printing bearings. Polyjet printing yields more accurate dimensions than FDM printing. Using these printing techniques, four bearing configurations are tested: PLA Flexure Pivot, Photopolymer Flexure Pivot, Photopolymer Plain Journal and Photopolymer Pressure dam.

In terms of static response:

- For plain journal bearing, the measured flow rate is higher than predicted for all cases. The predictions follow the same trend as the measured results, flow increases with speed and load. Predicted temperature rise in the PJB was much higher than measured. The trend of the predicted values is the same as the measured results, temperature rise increases with speed and decreases with load. The under prediction of the flow rate may explain the over prediction of the temperature rise.
- Predicted flow rates in the pressure dam bearing is higher than what was measured for all test conditions. Flow rate increases with speed for both predicted and measured values, however, the predicted values do not significantly change with load. The predicted temperature rise is reasonably close to the measured values. Temperature rise predicted and measured values both increases with speed, however, the predicted values do not change with load.

In terms of vibration response, results show:

- Pressure dam bearing provides the best performance in term of vibration at 2000, 5000, and 8000 rpm among the 4 bearings.
- @2000rpm, the journal bearing operates poorly while at above 5000rpm, photopolymer flexure pivot bearing experience instability for low load operating condition.
- Due to an effect of split critical speeds, photopolymer helps to bring down the max vibration at critical speed while pressure damp bearing helps to narrow down the speed band at critical speed condition.

This is tabulated in the table below.

	Load (N)	Vibration amplitude (mils pk-pk) @2000 rpm	@5000 rpm	@8000 rpm	Critical speed	Sign of instability
Flexure pivot (PLA)	**0**	0.75	2.5	2.75	4.5mils @2400rpm	yes. Start @5000rpm
	2	1	2.5	2.5	5mils @2400rpm	no
	4	1	1.5	2	5mils @2400rpm	no
	6.5	1	2	2	5mils @2400rpm	no
Flexure pivot (photopolymer)	**0**	2	4	4	split: 3mils @2000rpm & 3.75mils @2500rpm	yes. Start @5000rpm
	2	1	1.5	3	split: 1.25mils @1850rpm & 2.5mils @2400rpm	yes. Start @8000rpm
	4	0.75	1.5	2	split: 1.25mils @1900rpm & 1.5mils @2400rpm	no
	6.5	1	2	2.5	3.5mils @2500rpm	no
Plain journal (photopolymer)	**0**	3	2	2.25	7mils @2400rpm	no
	2	2	2	2	5mils @2400rpm	no
	4	1.5	2	2	6mils @2400rpm	no
	6.5	1	1.5	1.5	5mils @2400rpm	no
Pressure dam (photopolymer)	**0**	0.75	1.75	1.5	5mils @2350rpm	no
	2	0.5	1.75	2	6mils @2400rpm	no
	4	0.75	1.5	1.5	5.5mils @2400rpm	no
	6.5	1	1.75	1.75	5mils @2400rpm	no

The objectives of this study were met. However, the results show that there are many questions unanswered, which open possibility of future work in this area.

References

[1] idea_beans, “Spinning Triple/Quadruple Ball Bearings by idea_beans,” *thingiverse*. [Online]. Available: http://www.thingiverse.com/thing:51806. [Accessed: 04-Dec-2016]

[2] G. Reininger, “3D-printed Bearings: Less material = less weight - Franke Innovativ,” *Franke Innovativ*. [Online]. Available: http://www.franke-innovativ.com/3d-printed-bearings-less-material-less-weight/. [Accessed: 04-Dec-2016]

[3] M. Abrams, “3D Printing for Mass Production,” *The American Society of Mechanical Engineers*, Feb-2015. [Online]. Available: https://www.asme.org/engineering-topics/articles/manufacturing-processing/3d-printing-for-mass-production. [Accessed: 04-Dec-2016].

4] P. E. Allaire, J. C. Nicholas, and L. E. Barrett, “Analysis of Step Journal Bearings—Infinite Length, Inertia Effects,” *ASLsE Transactions*, vol. 22, no. 4, pp. 333–341, 1979.

[5] J. C. Nicholas and P. E. Allaire, “Analysis of Step Journal Bearings—Finite Length, Stability,” *ASLE Transactions*, vol. 23, no. 2, pp. 197–207, 1980.

[6] P. E. Allaire and R. D. Flack, “DESIGN OF JOURNAL BEARINGS FOR ROTATING MACHINERY,” in *Tenth Turbomachinery Symposium*.

[7] San Andrés, L., 2006, “Hybrid Flexure Pivot-Tilting Pad Gas Bearings: Analysis and Experimental Validation,” *J. Tribology*, 128(3), pp. 551-558

[8] D. J. Salamone, “JOURNAL BEARING DESIGN TYPES AND THEIR APPLICATIONS TO TURBOMACHINERY ,” in *THIRTEENTH TURBOMACHINERY SYMPOSIUM*.

[9] Texas A&M Engineering, “Stratasys 3D Printers | 3D Printing Studio | Current Students | Mechanical Engineering | College of Engineering,” *Stratasys 3D Printers | 3D Printing Studio | Current Students | Mechanical Engineering | College of Engineering.* [Online]. Available: https://engineering.tamu.edu/mechanical/current-students/3d-printing-studio/stratasys-3d-printers. [Accessed: 04-Dec-2016].

[10] “PolyJet Technology,” *PolyJet Technology | Stratasys*. [Online]. Available: http://www.stratasys.com/3d-printers/technologies/polyjet-technology. [Accessed: 04-Dec-2016].

[11] “Material Extrusion | Additive Manufacturing Research Group | Loughborough University,” *Material Extrusion | Additive Manufacturing Research Group | Loughborough University*. [Online]. Available: http://www.lboro.ac.uk/research/amrg/about/the7categoriesofadditivemanufacturing/materialextrusion/. [Accessed: 04-Dec-2016].

[12] J. E. Gaines and D. W. Childs, “The Impact of Pad Flexibility on the Rotordynamic Coefficients of Tilting-Pad Journal Bearings,” *Volume 7A: Structures and Dynamics*, 2015.

[13] E. Wilcox, “Troubleshooting Turbomachinery Using Start-up and Coast Down Vibration data,” in *Thirty First Turbomachinery Symposium*.

Appendix

A. ISO VG 32 Properties

TYPICAL TEST DATA

ISO Grade	32	46	68	100
Product Number	*253026*	*253027*	*253028*	*253029*
SDS Number	*6710*	*6710*	*6710*	*6710*
AGMA Grade	—	1	2	3
API Gravity	32.7	32.0	31.7	31.4
Viscosity, Kinematic cSt at 40°C cSt at 100°C	 32.0 5.4	 43.7 6.6	 68.0 8.8	 100.0 11.4
Viscosity, Saybolt SUS at 100°F SUS at 210°F	 165 44.4	 225 48.2	 352 55.9	 520 65.4
Viscosity Index	102	101	102	100
Flash Point, °C(°F)	222(432)	224(435)	245(473)	262(504)
Pour Point, °C(°F)	-36(-33)	-36(-33)	-33(-27)	-30(-22)
Oxidation Stability ASTM D943[a] ASTM D2272[b]	 17,000 1700	 12,000 1400	 11,000 1400	 11,000 1400

a Hours to 2.0 mg KOH/g acid number modified D943, allowed to run beyond 10,000 h.
b Minutes to 25 psi pressure drop.

Minor variations in product typical test data are to be expected in normal manufacturing.

Figure 69 ISO VG 32 properties (taken from Chevron Data sheet)

B. Probe calibration

PROBE CALIBRATION REPORT

Channel	1

GAP(mils)	OUTPUT(Volts)
0	0.0000
5	2.0054
14.5	4.0031
23.5	6.0027
33.5	8.0020
44.5	10.001
53.5	12.001
61.5	14.025

Specification	200	mV/mil
Actual	199.95	mV/mil

Error	-0.03%

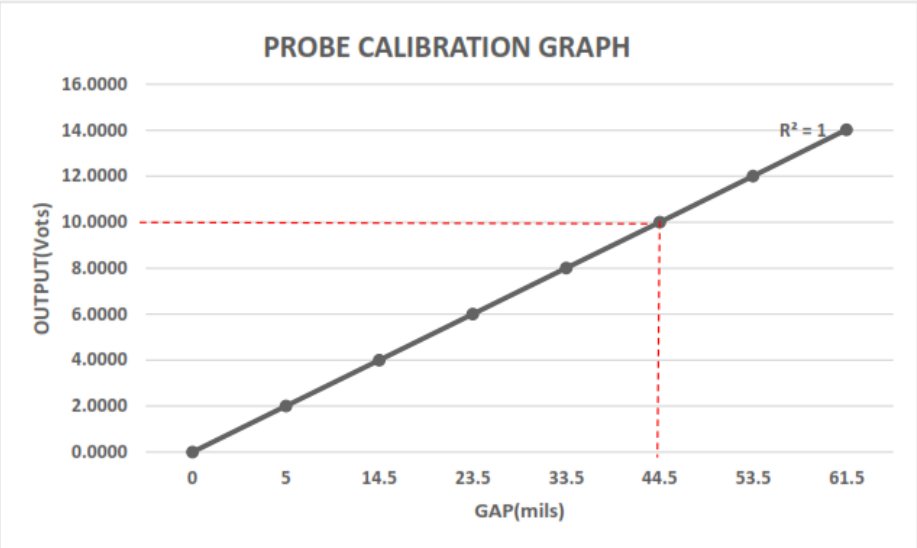

PROBE CALIBRATION REPORT

Channel	2

GAP(mils)	OUTPUT(Volts)
0	0.0000
9	2.0054
19	4.0000
28	6.0780
35	8.0700
45	10.0150
55	12.0100
63	14.0710

Specification	200	mV/mil
Actual	197	mV/mil

Error	-1.50%